MULTIFUNCTIONAL COATINGS ON TITANIUM SUBSTRATES FOR DENTAL IMPLANT APPLICATIONS

Maria del Mar Arrés Gonzalez

Thesis to obtain the Master of Science Degree in

Mechanical Engineering

Supervisors: Prof. Augusto Manuel Moura Moita de Deus
Prof. Catarina Ferreira dos Santos

Examination Committee

Chairperson: Prof. Luís Filipe Galrão Dos Reis
Supervisor: Prof. Augusto Manuel Moura Moita de Deus
Member of the Committee: Prof. Maria João Pedroso Carmezim

July 2018

To my grandmothers

Acknowledgements

Firstly, I would like to thank Prof. Catarina Ferreira dos Santos, Prof. Augusto Manuel Moura Moita de Deus and Prof. Maria de Fátima Reis Vaz for the continuous guidance and support throughout the duration of my work. In addition to their availability, their ability to guide me appropriately and give me conscious feedback has enhanced my research and findings which invariably has added a lot of value to my knowledge and without their support, the completion of this project would have been incomplete. In particular, I am thankful to Prof. Catarina Ferreira dos Santos for all the effort which was invested in this project and thanks to Prof. Augusto Manuel Moura Moita de Deus and Prof. Maria de Fátima Reis Vaz for trusting me from the beginning.

Additionally, I am thankful to all the IST professionals for always receiving me with sympathy and goodwill throughout the tests and the analysis of the data. I am also thankful to my colleagues Diogo Rechena, Pedro Costa and Hugo Araújo for their unconditional support and constant assistance and their inputs have helped me to complete this project efficiently.

Finally, I would also like to mention my support system i.e, all my colleagues and friends who have been supportive during this period. Also, thanks to my family especially my father, my sister and my boyfriend for their unconditional support and their constant motivation when I needed it the most. Also, for providing me with the crucial resources (financial support), and for believing me in my potential. Without them, this would not have been possible. Thanks for being always close by me.

Abstract

Titanium (Ti) has been extensively applied to orthopedic and dental implants due to its excellent physical and mechanical properties. However, its bioinert nature restrains its further uses. To address this, surface modification can be implemented to enhance its osteogenic activity. Hydroxyapatite (HAp) is a calcium phosphate material, with high bioactivity and biocompatibility, with composition and structure similar to the natural bone. HAp-coated dental implants have early bone response and a high interface shear strength. In recent years, many methods have been developed to deposit a HAp layer onto biomedical metal surfaces.

The aim of this work is to develop a nanostructured HAp coating on top of pure titanium. For that, different experimental conditions were studied and then the coatings were characterized using different physico-chemical techniques. Additionally the mechanical properties were evaluated using simulation, nanoindentation and bending test.

Hydroxyapatite was successfully synthesized on titanium substrate by hydrothermal method. The results showed that the presence of TiO_2 on titanium is a key factor inducing the growth of hydroxyapatite coating during the synthesis. According to SEM/EDS results and ATR-FTIR spectroscopy, HAp particles were present on all produced coatings. Additionally, in presence of TiO_2 and with 24 hours of hydrothermal process, the nanocoating was homogeneous, crack-free and adherent with uniform thickness.

On the other hand, from modelling results it is possible to corroborate the experimental results. Young's modulus value is reduced in presence of the coating. For a higher treatment time and in the presence of oxide layer, a higher Young's Modulus is obtained.

Keywords: Titanium, Hydroxyapatite coating, surface functionalization, hydrothermal method.

Resumo

O titânio (Ti) tem sido extensivamente utilizado em implantes ortopédicos e dentários devido às suas excelentes propriedades físicas e mecânicas. No entanto, devido ao fato de ser bioinerte, isso restringe o seu uso. Para resolver esse problema, a funcionalização da superficie levará a uma modificação da mesma e assim a uma melhor resposta osteogénica. Nesse respeito, a hidroxiapatite (HAp) é reconhecida como um dos materiais mais elegíveis e poderia ser potencialmente integrada com as vantagens do titânio para formar um revestimento compósito para usos versáteis, como implantes médicos. Eles de facto têm sido usados clinicamente por mais de dez anos. Os implantes dentários revestidos com HAp têm uma resposta óssea precoce e uma maior resistência às tensões de corte na interface com o osso. Em anos recentes, muitos métodos foram desenvolvidos para depositar uma camada de HAp numa superfície metálica em aplicações biomédicas.

Este trabalho pretende estudar a formação do revestimento de HAp em titânio puro, analisando as diferentes condições de formação, a caracterização do revestimento e as propriedades mecânicas do mesmo. O revestimento foi realizado por tratamento hidrotérmico, para cada condição. Os resultados obtidos permitem apoiar as investigações anteriores do revestimento de HAp em titânio sintetizado por tratamento hidrotérmico.

A hidroxiapatite foi sintetizada com sucesso em substrato de titânio pelo método hidrotérmico. Os resultados mostram que a presença de TiO_2 em titânio é um fator chave que induz o crescimento do revestimento de hidroxiapatite durante a síntese. De acordo com os resultados de SEM / EDS e espectroscopia de ATR-FTIR, partículas de HAp estavam presentes em todos os revestimentos produzidos. Além disso, na presença de TiO_2 e com 24 horas de processo hidrotérmico, o nanorevestimento é homogêneo, livre de fendas, aderente e com espessura uniforme.

Por outro lado, a partir de resultados de modelação é possível corroborar os resultados experimentais. O valor do módulo de Young é reduzido na presença do revestimento. Para um tempo de tratamento mais elevado e na presença de camada de óxido, obtém-se um módulo de Young maior.

Palavras-chave: Titânio, revestimento de hidroxiapatite, funcionalização da superfície, método hidrotermal.

Index

1. Introduction ……1
   1.1 Motivation and background ……..……..2
   1.2 Objective ……..……...5
2. Materials and methods ……..……7
   2.1 Materials ……..……8
   2.2 Coating production ……..……..…..…..…10
   2.3 Surface characterization techniques ……..……....…11
      2.3.1 X-Ray diffraction ……..……...11
      2.3.2 SEM and FTIR-ATR ……..…..…….15
      2.3.3 Contact angle ……..……...……...…..…….18
      2.3.4 AFM ……..……..…….20
   2.4 Mechanical techniques ……..……..…..…22
      2.4.1 Nanoindentation test ……...22
      2.4.2 Bending test ……..……...24
      2.4.3 Finite element analysis ……..……...25
3. Results and discussion ……27
   3.1 Physical-chemical characterization ……..……...…28
      3.1.1 Effect of the presence of titanium oxide layer on coating morphology ….....28
      3.1.2 Effect of the synthesis time ……...39
      3.1.3 Summary ……...……...…...44
   3.2 Mechanical testing and modelling ……..……..…45
      3.2.1 Indentation ……..……..45
      3.2.2 Bending ……..……..……..……...48
      3.2.3 FE modelling ….....……...…...50
4. Conclusions and future work ……..……..……55
   4.1 Conclusions ……..……....56
   4.2 Future work ……....……...…57
   References ……..……58

List of figures

Fig 2.1. Titanium used in this study: a) pure titanium b) with coating ……..……..…....9

Fig 2.2. Titanium rods used in the bending test ……..……..….9

Fig 2.3. Schematic view of HAp-coating formation under hydrothermal conditions…....……10

Fig 2.4. Schematic representation of X-Ray diffraction…….....…..……..11

Fig 2.5. XRD patterns of the samples after hydrothermal synthesis in 220°C for 7 h on: (a) acid etched Ti substrate, (b) 400 °C and (c) 650°C ……...……..…..….12

Fig 2.6. Characteristic plots of the different types of crystal phases: (a) anatase, (b) rutile …….....13

Fig 2.7. Bruker's X-ray Diffraction D8-Advance instrument. ……..……14

Fig 2.8. SEM components ……15

Fig 2.9. SEM microscopy device ……..……...……15

Fig 2.10. FTIR spectrum of nanocomposite HAp/TiO_2 coating ……..……..…….17

Fig 2.11. FTIR-ATR spectrometer ……..……..…...17

Fig 2.12. Representation scheme of determination of contact angle ……...…….18

Fig 2.13. Optical system device ……..……...……19

Fig 2.14. AFM explanation 20

Fig 2.15. Atomic force microscopy ……..……..21

Fig 2.16. Example of nanoindentation curve (sample TI24O): force (mN) vs. depth (μm) ……22

Fig 2.17. Dynamic ultra-micro hardness test ……...……...23

Fig 2.18. Instron model bending test in R4 ……...24

Fig 2.19. FE model in 3D ……...25

Fig 2.20. Boundary conditions representation ……..……..……..26

Fig 3.1.1.. SEM images of the calcium phosphate coating synthesized after 6 hours in (a, b) (Ti6NO) absence of titanium oxide layer, (c, d) (Ti6O) in presence of titanium oxide layer……..…..29

Fig 3.1.2. AFM pictures at 1μm of titanium and titanium coated with calcium phosphate in presence and absence of oxide layer at 6 hours ……...……..…..30

Fig 3.1.3. AFM pictures at 4µm of titanium and titanium coated with calcium phosphate in presence and absence of oxide layer at 6 hours ……..….30

Fig 3.1.4. EDS analysis of calcium phosphate coating on pure titanium at 6 hours (a) without oxide layer, (b) with oxide layer ……..……..…..31

Fig 3.1.5. SEM picture of calcium phosphate coating (a) without and (b) with oxide layer; EDX maps of calcium, phosphorus, oxygen and titanium elements respectively (c, d; e, f; g, h; i, j) ……..…..…32

Fig 3.1.6. FTIR results corresponding to pure titanium and HAp coating obtained by hydrothermal process: magnification of the 600-1600 cm^(-1) spectral region ……..……..32

Fig 3.1.7. FTIR results corresponding to pure titanium and HAp coating obtained by hydrothermal process: magnification of the 1000-1300 cm^(-1) spectral region ……33

Fig 3.1.8. FTIR results corresponding to pure titanium and HAp coating obtained by hydrothermal process: magnification of the 1300-2000 cm^(-1) spectral region ……33

Fig 3.1.9. XRD patterns of (a) pure titanium, (b) calcium phosphate synthesized on titanium with and without oxide layer ……35

Fig 3.1.10. XRD patterns from 25º to 45º of (a) pure titanium, (b) CP synthesized in 6 h on Ti without oxide, (c) CP synthesized in 24 h on Ti without oxide layer, (d) CP synthesized in 6 h on Ti with oxide and (e) CP synthesized in 24 h on Ti with oxide layer ……36

Fig 3.1.11. SEM picture of coating without oxide in Ti24NO ……..……..……37

Fig 3.1.12. SEM picture of coating with oxide in Ti6O ……..……..37

Fig 3.1.13. Static contact angle measurements on pure titanium and HAp coatings in plane samples ……38

Fig 3.1.14. SEM images of the calcium phosphate coating synthesized after 24 hours and without oxide layer (a, b) (Ti24NO) and in presence of titanium oxide layer (c, d) (Ti24O) ……..……..……39

Fig 3.1.15. AFM pictures at 1µm of titanium and titanium coated with calcium phosphate in presence and absence of oxide layer at 24 hours by hydrothermal treatment ……40

Fig 3.1.16. AFM pictures at 4µm of titanium and titanium coated with calcium phosphate in presence and absence of oxide layer at 24 hours by hydrothermal treatment ……..……..40

Fig 3.1.17. EDS analysis of calcium phosphate coating on pure titanium at 24 hours (a) without oxide layer, (b) with oxide layer ……41

Fig 3.1.18. SEM picture of calcium phosphate coating at 24 hours (a) without and (b) with oxide layer; EDX maps of calcium, phosphorus, oxygen and titanium elements respectively (c, d; e, f; g, h; i, j) 42

Fig 3.1.19. Static contact angle measurements on pure titanium and HAp coatings in plane samples …....43

Fig 3.2.1. Young's Modulus results ……..……..……46

Fig 3.2.2. Berkovich hardness results ……..……..……..……46

Fig 3.2.3. Relation between force applied and displacement …….....……48

Fig 3.2.4. Relation between Relation between stress and strain ……..……48

Fig 3.2.5. Bending test in R4 ……..……..……..…..49

Fig 3.2.6. Stress distribution in pure titanium rod ……..……50

Fig 3.2.7. Load-displacement plot in pure Ti rod from finite element analysis ……..……..50

Fig 3.2.8. Von Mises stress- strain graph in pure Ti rod from finite element analysis ……..51

Fig 3.2.9. Stress distribution in a coated rod by finite element analysis ……51

Fig 3.2.10. Half view of stress distribution in the coated rod by finite element analysis ……52

Fig 3.2.11. Load-displacement graph in coated Ti rod from finite element analysis ……....52

Fig 3.2.12. Stress-strain plot in coated Ti from finite element analysis ……..……..……53

List of tables

Table 1. Composition of pure titanium used (impurity contents in ppm)……..……8

Table 2. Conditions and nomenclature used ……..……..……8

Table 3. Nomenclature and conditions of the rod samples ……....….24

Table 4. Mechanical properties definition ……25

Table 5. Summary of roughness ……..……41

Table 6. Summary conclusions of all the results ……..……..44

Table 7. Summary of values of relevant results ……..……..…..44

Table 8. Experimental values of Young's Modulus in pure titanium and in coated titanium ……..…49

Nomenclature

AFM: Atomic force microscopy

ATR: Attenuated total reflection

CP: Calcium phosphate ceramics

Cp-Ti: Commercially pure titanium

FEA: Finite element analysis

FTIR: Fourier-transform infrared spectroscopy

HAp: Hydroxyapatite

SEM: Scanning electron microscope

Ti: Titanium

TiO_2: Titanium oxide

XRD: X-ray diffraction

1 INTRODUCTION

Contents

1.1 Motivation and background ……

1.2 Objective ……

1.1. Motivation and background

In the last few decades there are has been an important growth in the different fields of medicine where advancements have occurred very fast, thanks to technological developments. The same is happening in the case of the field of implantology especially the treatment with dental implants [1].

Among the various metallic implants, commercially pure titanium (Cp-Ti) and its alloys are widely used as metallic biomaterials because of their good biocompatibilty and their good mechanical properties. This is due to its high corrosion resistance, flexibility (moderate modulus of elasticity), high resistance to attack of the corrosive ions present in the biological fluid, so its suitable mechanical properties along with biocompatible nature makes them indispensable in the field of orthopedics [2].

However, as biologically inactive materials, once implanted into the human body they get encapsulated by a fibrous tissue to isolate them from surrounding bone, which prolongs the healing time and may cause implant loosening [3].

Besides, pure Ti provokes adverse effects in the local tissues, because of the increased release of toxic, allergic and potentially carcinogenic ions, thus Ti is not recommended as the ‘‘golden standard’’ for osteosynthesis material [4].To overcome this problem surface implants functionalization could play an important role in achieving rapid stability and enhancing the bone-to-implant contact, reducing the total treatment time required [5].High requirements for dental and orthopedic implants have pushed the research towards new coatings. To overcome the disadvantages of a single phase implant, such as low biocompatibility for metals and poor mechanical properties for ceramics, a significant amount of research has been recently focused on the development of their combination, i.e. covering load-bearing metallic implants with thin bioactive ceramic-like films.

On the other hand, calcium phosphate ceramics, like hydroxyapatite (HAp) and bioactive glasses, have better compatibility to hard tissue than titanium. In the 1980s, HAp-coated implants received much attention mainly because of their biocompatibility [2].

Special interest has recently been paid to coating dental implants with hydroxyapatite (HAp). This is due to HAp-coated implants showing higher survival rates and an earlier bone response than commercial pure-titanium and titanium-alloy implants [5].

It is known that one main reason for the excellent physical and biological properties of pure titanium and its alloys is the spontaneously formed oxide film (TiO_2) that is created on its surface upon air exposure. This film, having only a few nanometers of thickness (4.3 ± 0.2 nm for the mechanically polished Cp-Ti surface), appears to be responsible for the chemical stability, chemical inertness, corrosion resistance, and even biocompatibility of titanium [6]. Moreoverver, the presence of titanium oxide has some benefits because hydroxyapatite coating (HAp coating) alone has some disadvantages such as (i) low melting point of phosphorous in the coating causing bioactive degradation of the coating (ii) the HAp coated implants giving a better pinning to the bone compared with that of the adhesion between coating and the implant which will ultimately lead to loosening and

failure of the implant. TiO_2 improves bioactivity and adherence of the coating to the substrate and also to the bone [7].

Hydroxyapatite (HAp) $[Ca_5(PO_4)_3OH]$ coatings have been studied for a long time. According to the literature the HAp coatings increases the bioactivity of the implant due possessing similar chemical, structural and biological properties to the human bone. More recently nanostructured coatings have been developed. The major advantage associated with nanostructured HAp coatings is that the nanoparticles present on titanium surface are similar (shape and size) to that of inorganic molecules of the human bone [8]. The structural similarity bone bonding capability, osteoconductivity and biocompatibility of HAp with the hard bone tissues makes HAp an attractive coating material to accelerate bone growth around the implant.

It is known that HAp-coated surfaces exhibit excellent tissue response and osteoconductivity without interfering in the mechanical properties of the implant material. Therefore, HAp-coated Ti implant can be an ideal candidate for an implant device. Coating of HAp layer on Ti implants was considered as a way of promoting osseointegration and overcoming the drawbacks of HAp [7]. *In vivo* studies achieved good results with respect to both bone adaptation to HAp-coated implants [9] and the binding strength of HAp-coated implant-bone interfaces [10,11].

Many methods have been developed to deposit a HAp layer onto a biomedical metal surface, including plasma spraying, sputtering process, sol–gel method, pulsed laser deposition, electrophoretic deposition, electrochemical deposition and hydrothermal synthesis [3]. Among them, plasma spray HAp is the most accepted and extensively clinically used method. However, the layer produced by this method is limited by: poor uniformity in coating thickness and in its adherence to substrate, phase inhomogeneity, low crystallinity, as well as degradation of bending strength and fatigue life caused by the dissolution of HAp phase in long-term contact with body fluids. In fact plasma spraying, a high temperature process, has difficulty in controlling the composition and crystallinity of the HAp layer [3]. Other techniques are sputtering and electrochemical deposition, which are also commercially applied but where the operation is complex and high-cost. Also, phase-pure and crystalline coatings were seldom obtained through these methods. Recently, another approach has been developed to form a highly crystalline HAp coating on Ti, namely by the hydrothermal method [12].

An ideal calcium phosphate coating should have strong surface attachment, proper coating coverage, and a simple processing method. The hydrothermal method presents a simple, inexpensive and environment friendly procedure to synthesize thin (or thick) shaped and homogeneous ceramic films and coatings in aqueous solutions in a one-step process for a variety of applications.

The synthesis is based on a chemical precipitation from an aqueous solution containing calcium and phosphate sources, carried out in an autoclave at elevated temperature and high vapor pressure. An organic modifier is often added, usually a chelating agent such as carboxylic acid or ethylenediamine tetraacetic acid (EDTA), to control supersaturation of HAp and thus the crystal growth rate. It's usually

added citric acid in order to get the same benefits. Upon heating, calcium chelate decomposes and calcium ions are slowly and continuously released so that the degree of supersaturation is constantly low during the deposition process [3].

Moreover, hydrothermal process is one excellent method for synthesizing crystalline coatings onto different substrates. However, single step hydrothermal requires high roughness of the substrate surface. Also, a high temperature is always used to annealing-treat the metal substrate and it could possibly cause damage and undesired by-products [4].

On the other hand, as a result of hydrothermal process, micro-sized roughness forms and remains almost unchanged after the annealing. This fact leads to a conclusion, that roughness of the substrate is not the critical parameter intensifying the HAp nucleation during the hydrothermal synthesis [3].

Bibliography reported that hydrothermal treatment in CaO solution enhanced the precipitation of apatite on the titanium surface. Also some studies proposed that Ti-O-Ca boding formed by hydrothermal treatment in $CaCl_2$ solution is effective for the fabrication of titanium implant with good bioactivity and osteoconductivity. In addition they referred to a one step hydrothermal process (instead of two steps) with hydroxyapatite (HAp) suspension to coat Ti surface [13].

Hydrothermal coating method has been used to coat Ti. For that, it was reported the use of a solution with Ca^{2-} (0.2 M) and $(NH_4)_2HPO_4$ (0.12 M) and a temperature of 220ºC for 7h. The authors reported that a well-crystallized HAp coating was produced with a thickness of 170 µm and with good adhesion [3].

Another important aspect is that hydrothermal coating method allows the production of HAp coatings with a Ca/P ratio close to the stoichiometric value. As mentioned before, this method is easy to perform, since it doesn't require much time and the cost is low.

Regarding to the coating benefits, coating of Ti surfaces with calcium phosphate nanostructures can improve soft tissue integration and osteogeneration that leads to improved fixation of implants. Furthermore, osteoconductive nanostructures induce a chemical bond with bone to attain good biological fixation for implants [14].

When the thickness of coatings obtained by hydrothermal method is above 150 µm, the HAp coatings would not be useful for clinic application. According to the literature, the thickness of Hap coatings on dental implant is in the range of 60–120 µm have more satisfactory biological response [15]. For this reason, we focus on obtaining the thickness lower than 80-170 µm, which is the range obtained until now in previous investigations [3].

Regarding to mechanical properties, dental implants are subjected to many cycles during mastication, which may break them. Investigation of the stress distribution can provide important information for implant design and optimizing implant placement for various types of bone quality. It is known that the success of dental implants depends on the manner in which stresses are transferred to the surrounding bone. Load transfer from implants to surrounding bone depends on the type of loading,

the bone to implant interface, the length and diameter of the implants, the shape and characteristics of the implant surface, the prosthesis type, and the quantity and quality of the surrounding bone. Implant design features are one of the most fundamental elements that have an effect on implant primary stability and ability of implant to sustain loads during or after osseointegration [16].

Despite its numerous benefits, HAp coating has a main disadvantage i.e. the high risk of crack formation at the interface of the coating layer and the dental implant. This is due to sudden change of mechanical properties at the interface and possibly undesirable deficiencies during the manufacturing process [17].

Low bonding strength and sudden variation of mechanical properties between the coating and the metallic layers are the main disadvantages of such common implants [17]. To address these problems, in this section will be study the effect of a coating on mechanical properties by means of the three-point bending test (coating and pure titanium), as well as study the stress distribution in the sample during the test.

Finite element analysis (FEA) is a technique for obtaining a solution to a complex mathematical problem by dividing the problem domain into a collection of much smaller and simpler domains or elements in which the field variables can be interpolated with the use of simple shape functions. In another words, FEA is a method whereby, instead of seeking a solution function for the entire domain, one formulates the solution functions for each finite element and combines them properly to obtain the solution to the whole body [16].This method can be used to study the stress distribution in these systems.

1.2. Objective

The strategy proposed in the present work is the functionalization of titanium surface with a calcium phosphate nanostructured coating. For that the hydrothermal coating process will be used. It will also evaluate coating features, such as composition, morphology, thickness, wettability, and Young's modulus in different experimental conditions namely: synthesis time and presence of oxide titanium.

The hydrothermal method will be used with the objective of to obtain in one unique step the calcium phosphate coating.

On the other hand, in this study the bending test will be performed in order to evaluate the mechanical response of the coated material; and a parallel study by means of finite element analysis (FEA) will be done, in order to better understand the possible effect of the coated layer on the overall mechanical behavior.

2 MATERIALS AND METHODS

Contents

2.1 Materials ………………………………………………………………………………………………….....
2.2 Coating production ………………………………………………………………………………………
2.3 Surface characterization techniques …………………………………………………………………......
2.3.1 X-Ray diffraction ………………………………………………………………………………………
2.3.2 SEM and FTIR-ATR …………………………………………………………………………….......……
2.3.3 Contact angle …………………………………………………………………………………………….
2.3.4 AFM ……………………………………………………………………………………………………….
2.4 Mechanical techniques ……………………………………………………………………......………….
2.4.1 Nanoindentation test ……………………………………………………………………………………
2.4.2 Bending test ……………………………………………………………………………………………
2.4.3 Finite element analysis ……………………………………………………………………………

2.1. Materials

Four disk-shaped pure Ti plates with 16 mm in diameter and 1-2 mm in thickness were cut from commercial bars by an automatic cutting machine. The composition of titanium is presented in table 1:

Table 1. Composition of pure titanium used (impurity contents in ppm)

Titanium	Matrix
Aluminium	2.5
Calcium	< .2
Carbon	26.5
Chromium	18
Cobalt	0.4055
Copper	1.1
Iron	12.5
Manganese	0.2025
Mercury	< .1
Nickel	0.14
Niobium	< .2
Rhodium	< .15
Rubidium	< 5
Silicon	1
Tantalum	< 5
Vanadium	0.35
Yttrium	<200
Zirconium	0.6

To produce the calcium phosphate coating some titanium substrates were polished immediately before been introduced on autoclave and others were left in contact with air during 24 hours. The Ti was polished using a SiC abrasive papers with roughness 800 and 1000. After that the polished titanium was washed with water and acetone in order to remove small particles, and dried.

To evaluate the effect of the synthesis time on coating characteristics the pure titanium was functionalized in an autoclave for 6 and 24 hours. In this study the following nomenclature will be used and it's presented in table 2:

Table 2. Conditions and nomenclature used

Nomenclature	**Conditions**	
Ti6NO	6 h	Absence of TiO_2
Ti24NO	24 h	Absence of TiO_2
Ti6O	6 h	Presence of TiO_2
Ti24O	24 h	Presence of TiO_2

Figure 2.1 show pictures of titanium before and after the deposition process and in figure 2.2 the rods that are used in the mechanical test are presented.

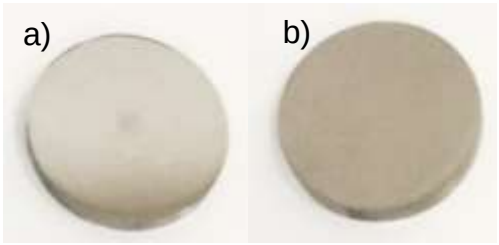

Fig 2.1. Titanium used in this study: a) pure titanium; b) with coating

Fig 2.2. Titanium rods used in the bending test

2.2 Coating production

The coatings formation was carried out by hydrothermal method. First it was prepared a 0.6 M citrate aqueous solution using a citric acid monohydrate ($C_6H_8O_7 \cdot H_2O, 99.5\%$).

After that, the pH of the solution was adjusted with ammonium hydroxide solution ($NH_4OH, 25\%$) until pH~8 was reached. Then 0.2 M of calcium nitrate tetrahydrate ($Ca(NO_3)_2 \cdot 4H_2O,\ 99\%$) was added to the solution.

Finally, a 0.2 M ammonium hydrogen phosphate aqueous solution ($(NH_4)_2HPO_4$) was added. Then, both solutions were mixed.

The prepared solution was put in Teflon vessels (50 ml) and then transferred to a stainless steel autoclave. The autoclaves were kept at 180°C during 6 h and 24 h.

After hydrothermal coating process, the autoclaves were cooled down and the Ti plates were removed from the autoclave, washed with distilled water and dried.

A schematic representation of the HAp coating formation is presented in figure 2.3:

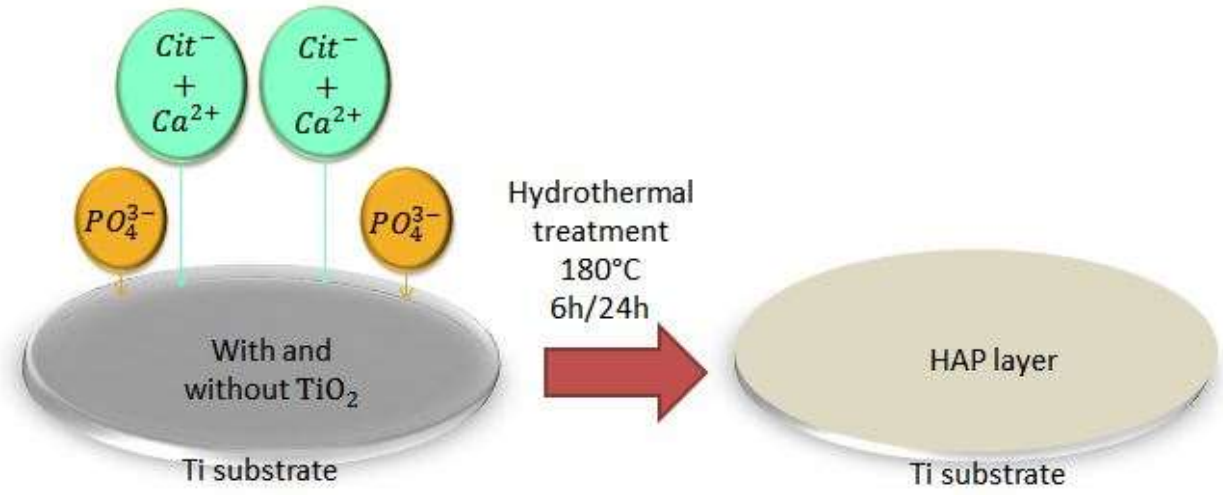

Fig 2.3. Schematic view of HAp-coating formation under hydrothermal conditions

2.3 Surface characterization techniques

2.3.1. X-Ray diffraction

Crystalline phases of the calcium phosphate coating were analyzed using a X-ray-diffractomer.

X-ray diffraction (XRD) relies on the wave nature of X-rays to obtain information about the structure of crystalline materials. A primary use of the technique is the identification and characterization of phases based on their diffraction pattern [18].

The dominant effect that occurs when an incident beam of monochromatic X-rays interacts with a target material is scattering of those X-rays from atoms within the target material. In materials with regular structure (i.e. crystalline), the scattered X-rays can undergo constructive interference.

The diffraction of X-rays by crystals is described by Bragg's Law and a scheme is presented in figure 2.4:

$$\mathbf{n\lambda = 2d\ sin(\theta)} \qquad \text{(eq. 1)}$$

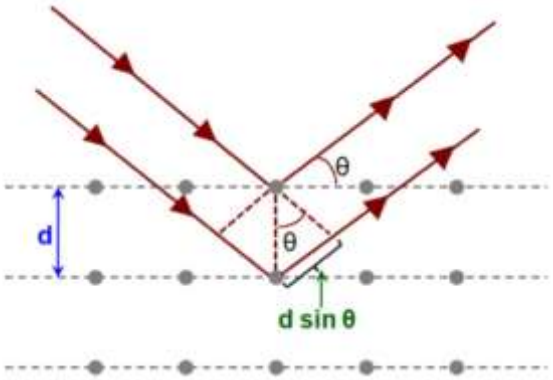

Fig 2.4. Schematic representation of X-Ray diffraction

The directions of possible diffractions depend on the size and shape of the unit cell of the material. The intensities of the diffracted waves depend on the kind and arrangement of atoms in the crystal structure. However, most materials are not single crystals, but are composed of many tiny crystallites in all possible orientations (ie polycrystalline aggregate) both in bulk or powder form. When a powder with randomly oriented crystallites is placed in an X-ray beam, the beam will see all possible interatomic planes. If the experimental angle is systematically changed, all possible diffraction peaks from the powder will be detected.

The parafocusing (or Bragg-Brentano) diffractometer is the most common setup for diffraction instruments.It offers the advantages of high resolution and high beam intensity analysis at the cost of very precise alignment requirements and carefully prepared samples. Additionally, this geometry requires that the source-to-sample distance be constant and equal to the sample-to-detector distance.

Alignment errors often lead to difficulties in phase identification and improper quantification. Sample flatness, roughness, and positioning constraints preclude in-line sample measurement.

X-ray diffractometers consist of three basic elements: an X-ray tube, a sample holder, and an X-ray detector.

The geometry of an X-ray diffractometer is such that the sample rotates in the path of the collimated X-ray beam at an angle θ while the X-ray detector is mounted on an arm to collect the diffracted X-rays and rotates at an angle of 2θ. The instrument used to maintain the angle and rotate the sample is termed a goniometer. For typical powder patterns, data is collected at 2θ from ~5° to 70°, angles that are preset in the X-ray scan.

The characteristic XRD spectra of hydroxyapatite coating obtained by hydrothermal method, titanium oxide and pure titanium it is presented in figure 2.5:

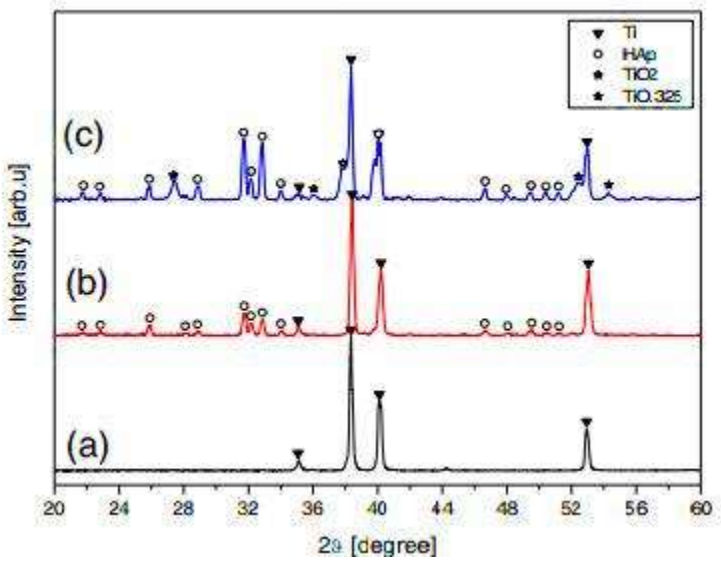

Fig 2.5. XRD patterns of the samples after hydrothermal synthesis in 220°C for 7 h on: (**a**) acid etched Ti substrate, (**b**) 400 °C and (**c**) 650°C [3]

On the other hand, two main crystalline forms of titanium dioxide can be considered: anatase and rutile. The characteristics difractograms of these phases are presented in figure 2.6 [19]:

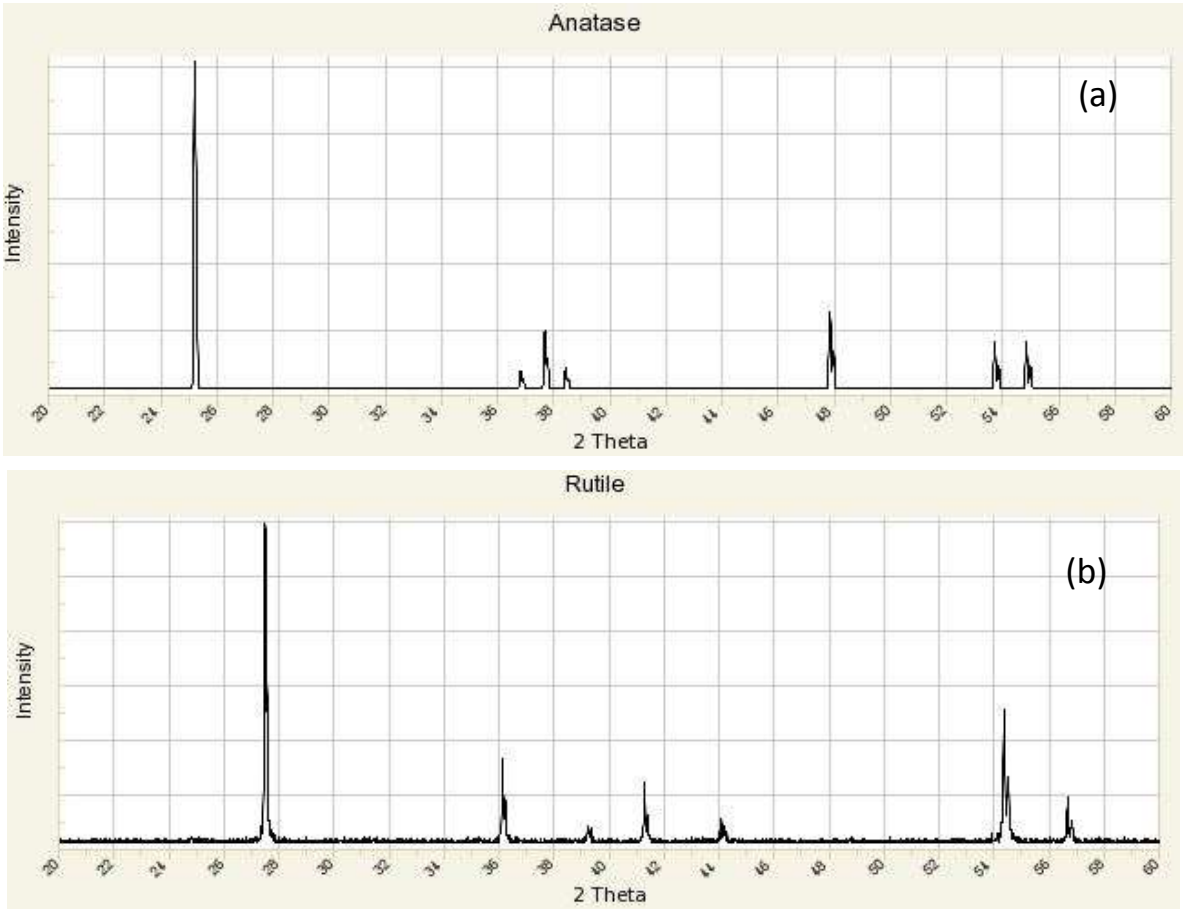

Fig 2.6. Characteristic plots of the different types of crystal phases: **(a)** anatase, **(b)** rutile

In this study, X-ray diffraction (XRD) analysis was done by a powder X-ray diffractometer (D8 Advance Bruker) with a CuKα radiation (ʎ=1.5406 Å) operated with a voltage of 40 kV and current of 40mA of tube current to identify the crystalline phase in the calcium phosphate coating. In addition a 0.5° grazing incident angle and scan rate at 0.02°step size from 5°-70° were applied.

Fig 2.7. Bruker's X-ray Diffraction D8-Advance instrument.

2.3.2. SEM and FTIR-ATR

Morphological and chemical composition evaluation of the calcium phosphate coating on Ti plate after hydrothermal process was performeded by scanning electron microscopy (SEM).

The scanning electron microscope uses a focused beam of high-energy electrons to generate a variety of signals at the surface of solid specimens. The signals that derive from electron-sample interactions reveal information about the sample including surface morphology, chemical composition, as well as crystalline structure [20].

The SEM is also capable to perform analyses of selected point locations on the material; this approach is especially useful in qualitatively or semi-quantitatively determining chemical compositions (using EDS). Figure 8 presents a scheme of the electron miscroscopy:

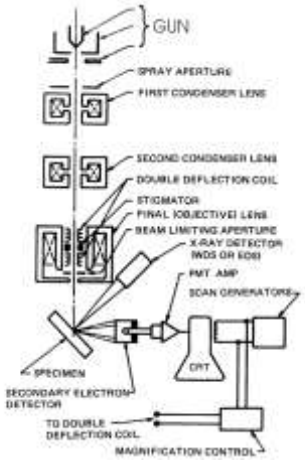

Fig 2.8. SEM components

The coated titanium samples were introduced inside the scanning electronic microscope (FEG-SEM JEOL 7001F)(figure 2.9) and the observation of the samples was done at 10 kV.

Fig 2.9. SEM microscopy device

Another technique used to analyze the chemical coating composition was Fourier-transform infrared spectroscopy (FTIR). When IR radiation is passed through a sample, some radiation is absorbed by the sample and some passes through (is transmitted). The resulting signal at the detector is a spectrum representing a molecular 'fingerprint' of the sample. The usefulness of infrared spectroscopy arises because different chemical structures (molecules) produce different spectral fingerprints [21].

Then, the Fourier Transform converts the detector output to an interpretable spectrum and the FTIR generates spectra with patterns that provide structural insights.

The FTIR uses interferometry to record information about a material placed in the IR beam. The Fourier Transform results in spectra that analysts can use to identify or quantify the material.

An FTIR spectrum arises from interferograms being 'decoded' into recognizable spectra. Patterns in spectra help identify the sample, since molecules exhibit specific IR fingerprints.

There are four major sampling techniques in FTIR:

- Transmission
- Attenuated Total Reflection (ATR)
- Specular Reflection
- Diffuse Reflectance

An ATR accessory operates by measuring the changes that occur in an internally reflected IR beam when the beam comes into contact with a sample. An IR beam is directed onto an optically dense crystal with a high refractive index at a certain angle. This internal reflectance creates an evanescent wave that extends beyond the surface of the crystal into the sample held in contact with the crystal.

In regions of the IR spectrum where the sample absorbs energy, the evanescent wave will be attenuated. The attenuated beam returns to the crystal, then exits the opposite end of the crystal and is directed to the detector in the IR spectrometer. The detector records the attenuated IR beam as an interferogram signal, which can then be used to generate an IR spectrum.

Figure 2.10 presents a characteristic spectrum of a HAp/TiO_2 nanocomposite coating:

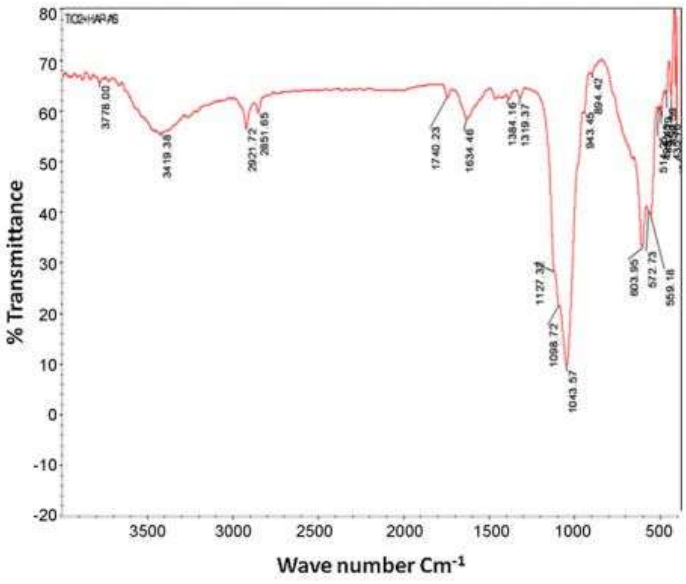

Fig 2.10. FTIR spectrum of nanocomposite HAp/TiO_2 coating [8]

The coated titanium samples were introduced inside the FTIR-ATR spectrometer (figure 2.11) and the test was done with a 4 cm^{-1} of resolution in transmittance format.

Fig 2.11. FTIR-ATR spectrometer

2.3.3. Contact angle

The characteristics of the surfaces are extremely important to evaluate the cell adhesion. To determine the wettability characteristics of the titanium before and after being coated, contact angle measures were done.

The contact angle is defined as the angle formed by a water drop when coming into contact with the substrate. The measurement and value of said angle will indicate the degree of wettability. Therefore, the contact angle is defined as the angle formed by the intersection of the liquid-solid interface and the liquid-vapor interface (geometrically acquired by applying a tangent line from the contact point along the liquid-vapor interface in the droplet profile). The interface where solid, liquid, and vapor co-exist is referred to as the “three phase contact line”.

Wettability studies usually involve the measurement of contact angles as the primary data, which indicates the degree of wetting when a solid and liquid interact. For contact angles greater than or equal to 90 ° we say that the adhesive does not wet the substrate, not generating adhesion between the adhesive and the substrate (hydrophobic); if the contact angle is lower than 90 ° we say that the adhesive wets the substrate generating adhesion between both materials (hydrophilic). That is, small contact angles (<90°) correspond to high wettability, while large contact angles (>90°) correspond to low wettability. More specifically, a contact angle less than 90° indicates that wetting of the surface is favorable, and the fluid will spread over a large area on the surface; while a contact angle greater than 90° generally means that wetting of the surface is unfavorable so the fluid will minimize its contact with the surface and form a compact liquid droplet [2].

According to Young's equation, there is a relationship between the contact angle θ, the surface tension of the liquid σ_l, the interfacial tension σ_{sl} between liquid and solid and the surface free energy θ_s of the solid [22]:

$$\theta_s = \sigma_{sl} + \sigma_l \cdot cos\theta \qquad \text{(eq. 2)}$$

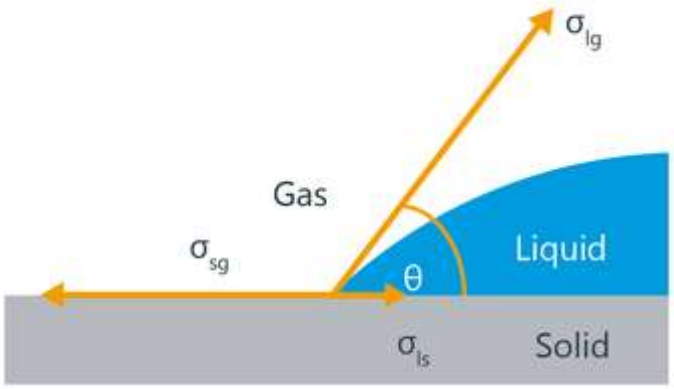

Fig 2.12. Representation scheme of determination of contact angle

In this study, a “goniometer” was used to measure contact angles (figure 2.13). This direct optical method is advantageous because of its simplicity and the fact that only small amounts of liquid (20 microliters) and small surface substrates (a few square millimeters) are required.

As for accuracy and reproducibility, the measurement relies on the consistency of the operator in the assignment of the tangent line, which can lead to significant error and inconsistency between multiple users.

In this work, four drops with 20 µl each were measured in contact with pure Ti, Ti6NO, Ti24NO, Ti6O and Ti24O. Then the obtained drop pictures were analyzed and the contact angle was obtained.

Fig 2.13. Optical system device

2.3.4. AFM

Atomic force microscopy (AFM) is a type of high resolution scanning probe microscopy that has a resolution that can be in the order of a nanometer. AFM uses a cantilever with a sharp probe that scans the surface of the specimen.

AFM includes a wide variety of methods in which the probe interacts with the sample in different ways in order to characterize various material properties. AFM can characterize a wide array of mechanical properties (e.g. adhesion, stiffness, friction, dissipation), electrical properties (e.g. capacitance, electrostatic forces, work function, electrical current), magnetic properties, and optical spectroscopic properties.

The heart of the AFM lies with the cantilever/tip assembly that interacts with the sample; this assembly is also commonly referred to as the probe. The AFM probe interacts with the substrate through a raster scanning motion. The up/down and side to side motion of the tip as it scans along the surface is monitored through the “beam deflection method”. The beam deflection method consists of a laser that is reflected off the back end of the cantilever and directed towards a position sensitive detector that tracks the vertical and lateral motion of the probe. The deflection sensitivity of these detectors has to be calibrated in terms of how many nanometers of motion correspond to a unit of voltage measured on the detector. This process is presented in figure 2.14.

In this study, static mode was performed in the samples. Static mode, or contact mode, is the original and simplest mode to operate an AFM. In this mode, the probe is in continuous contact with the sample while the probe raster scans the surface. In other words, the probe "drags" across the sample. The most common configuration of static mode is to operate it in constant force or deflection feedback mode. In this mode, the cantilever deflection is the feedback parameter. The cantilever deflection is set by the user and is related to how hard the tip pushes against the surface so that the user controls how gentle or aggressive the interaction between the probe and the sample is.

Static mode can also be operated in constant height mode where the probe maintains a fixed height above the sample. There is no force feedback in this mode. Constant height mode is typically used in atomic resolution AFM, though it is uncommon for other AFM applications.

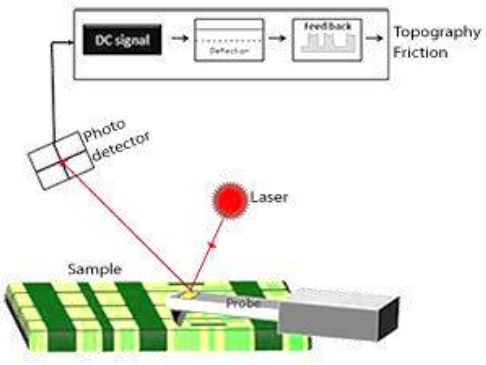

Fig 2.14. AFM explanation

The figure 2.15 shows the devices used to perform this test:

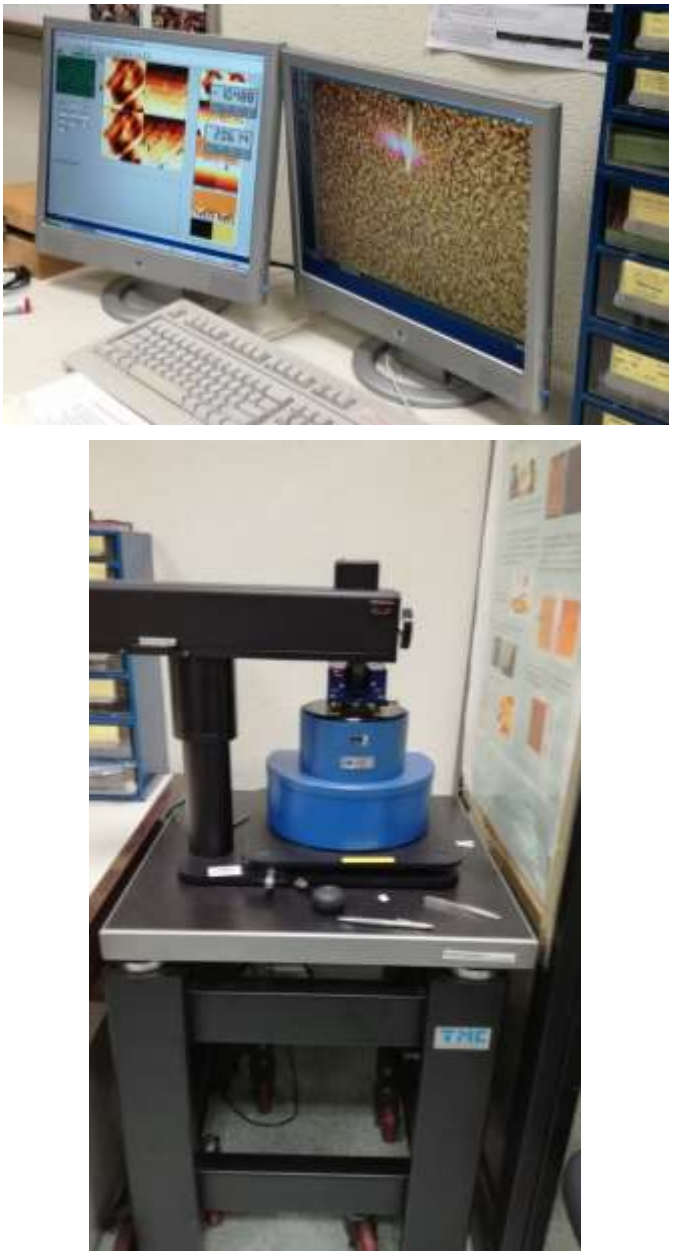

Fig 2.15. Atomic force microscopy

2.4. Mechanical techniques

2.4.1. Nanoindentation test

The principal components in a nanoindentation experiment are the test material, the sensors and actuators used to apply and measure the mechanical load and indenter displacement, and the indenter tip. The latter component is conventionally made of diamond whit a symmetric shape such as the three-sided Berkovich pyramid.

Nanoindentation provides a useful tool for determining mechanical properties such as the hardness, elastic modulus and fracture toughness of small samples.

During a typical nanoindentation test, force and displacement are recorded as the indenter tip is pressed into the test material's surface with a prescribed loading and unloading profile. The response of interest is the load-displacement curve (often called the P-h curve). The global shape of the P-h curve differs from one material to the next, and these variations usually reflect different mechanical properties. The following figure shows us an example when the force is load and then unloads.

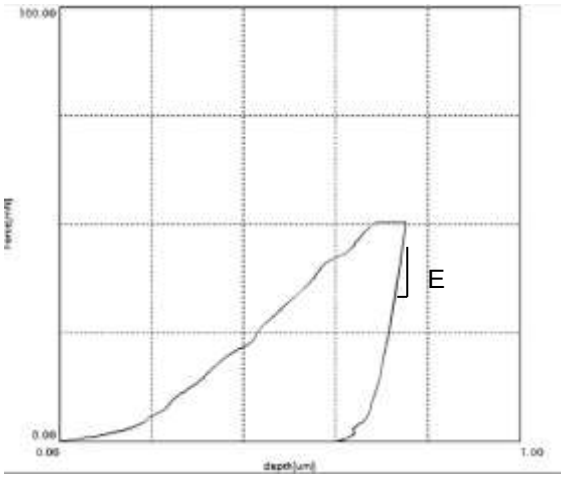

Fig 2.16. Example of nanoindentation curve (sample TI24O): force (mN) vs. depth (μm)

The conditions of nanoindentation testing used in this work are: load-unload test mode, 0.2-50 mN test force, 2 loading speed (6.66 mN/s), Poisson's ratio of 0.3 and hold time 15 s.

In figure 2.17 the device used in this test is presented:

Fig 2.17. Dynamic ultra-micro hardness test

2.4.2. Bending test

Bending tests deform the test material by means of the application of a bending moment and are typically performed to determine the stiffness or resistance to fracture of that material. The test sample is loaded in a way that creates a concave surface at the midpoint with a specified radius of curvature according to the standard in relation to which the test is performed. Bending tests are as common as tensile, compression, and fatigue tests. Bend testing a material allows for the determination of that materials stiffness, bend strength, fracture strength and resistance to fracture. These characteristics can be used to determine whether a material will fail under a given loading and are especially important in any construction process involving materials loaded with bending systems of forces. If a material begins to fracture or completely fractures during a three or four point bend test it is valid to assume that the material will fail under a similar loading in any application, which may lead to catastrophic failure [23].

In this section, we have used an universal testing system Instron Model 3369 of 50kN capacity. This test is carried out in rods of 32 mm length and 4 mm diameter. It is fixed in a support span of 16 mm. This test is carried out in five rods with the following nomenclature and conditions:

Table 3. Nomenclature and conditions of the rod samples

R1, R2 and R3	R4 and R5
24 h	Pure titanium
TiO_2	TiO_2

On the other hand, stress-strain curves can be built according to the following equations [33]:

$$\sigma = \frac{L*s}{\pi\left(\frac{d}{2}\right)^3}\ (MPa) \qquad \text{(eq. 3)}$$

$$\varepsilon = \frac{12\left(\frac{d}{2}\right)\Delta l}{s^2} * 100\ (\%) \qquad \text{(eq. 4)}$$

Where σ- stress (MPa); L=load (N); s=support span (mm); d=diameter of sample (mm); ε=strain (%); Δl=displacement (mm).

Fig 2.18. Instron model bending test in sample R4

2.4.3. Finite element analysis

In this study, an objective is to compare the results of the bending test (values of force and deformation applied to each sample) with the respective results obtained in Abaqus finite element simulations. With FEA we can get the force, stress and deformation in each node of the sample and the support beams. Similarly to the bending test, t force vs. displacement can be obtained, as well as the stress and deformation.

In addition, FEA is used in this work to better understand the effect of the film on the mechanical response of the coated part. In it, 3 rigid beams were designed to act as supports and to exert the load on the sample. The implant was simulated as a cylindrical rod since in the experimental test the sample that was used had this geometry. The main part has been divided in sections in order to improve the analysis of the results. The coating was defined like a cylindric shell with 100 µm of thickness, because it is the minimum possible value that was achieved without obtaining errors in the simulation (being a 2D mesh the dimension of the shell is very low comparing with the dimensions of the main rod [24]).

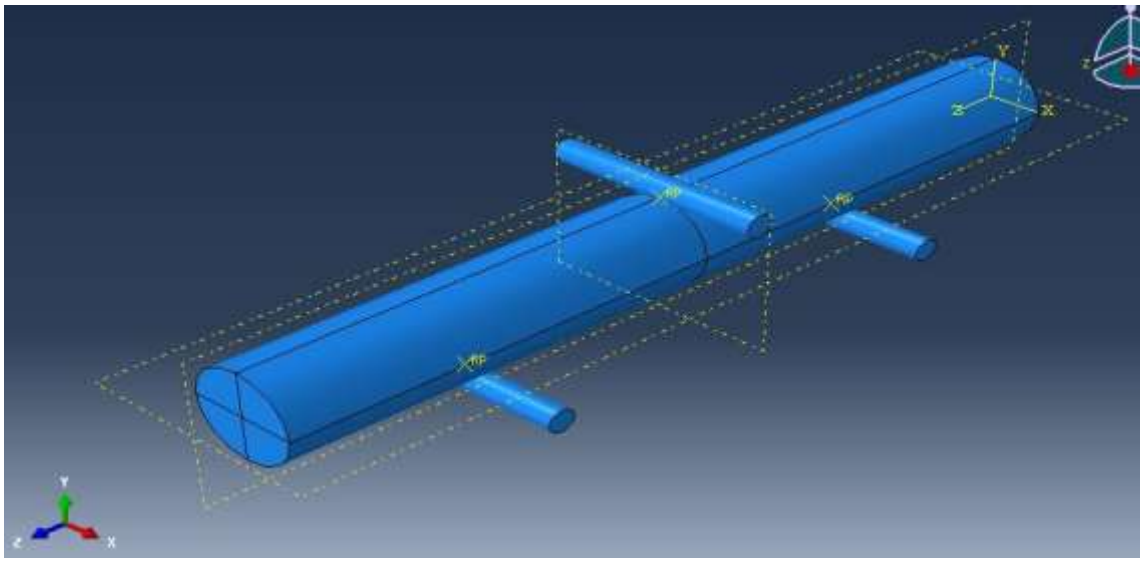

Fig 2.19. FE model in 3D

The mechanical properties of the structural materials (titanium and hydroxyapatite coating) were defined according to the literature [25]. They are presented in the table 4:

Table 4. Mechanical properties definition

	Titanium grade 4	Coating	Steel Supports
Young's modulus [GPa]	100	40	(rigid)
Poisson`s ratio	0.3	0.3	0.3

In order to avoid numerical errors, the supports were defined with a high Young's modulus value instead of a rigid solid in the part characterization. Regarding to the interaction, a friction coefficient of 0,2 was a used in the tangential contact.

Also, the following boundary conditions were considered and presented in figure 2.20:

i. The displacement of the beam on the top was imposed with a value of 1 mm vertically in order to analyze the stress distribution afterwards, as well as the reaction force caused by the rod. No applied load is defined.
ii. Supports are pinned; there is no movement in any axis.
iii. Nodes of the longitudinal section of the main rod are fixed in axis X, that allow displacement vertically (Y) and horizontally (Z).
iv. Nodes in the circular section of the mid-section of the rod are restricted to direction Z. It means that the material can deform in this plane, but without movement along the bar.

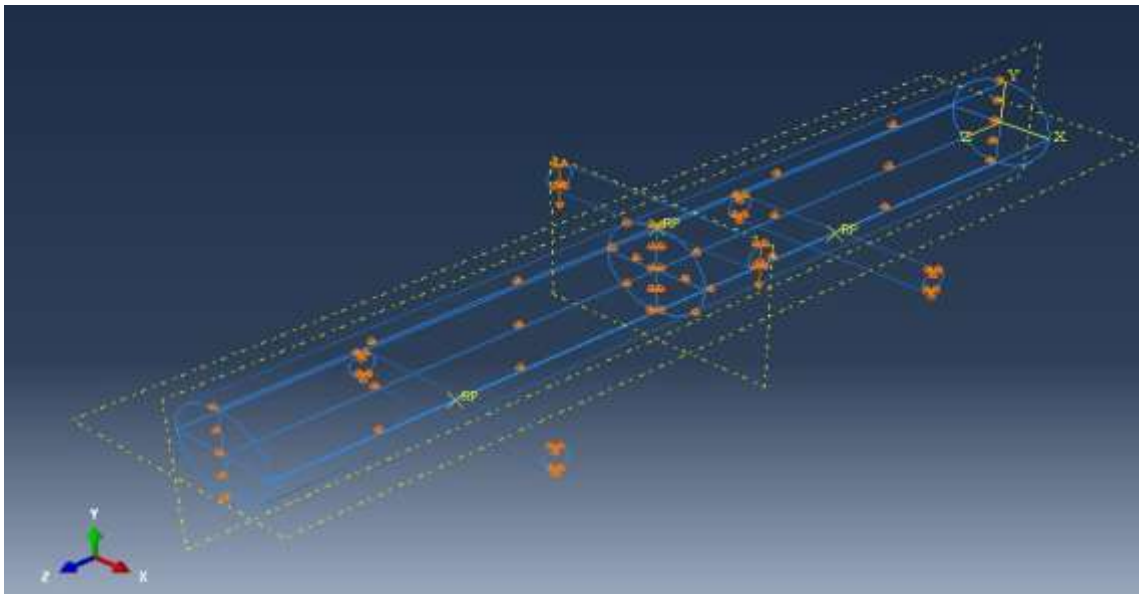

Fig 2.20. Boundary conditions representation

3 RESULTS AND DISCUSSION

Contents

3.1 Physical-chemical characterization ……..

3.1.1 Effect of the presence of titanium oxide layer on coating morphology…..……..……

3.1.2 Effect of the synthesis time……..……..……

3.1.3 Summary ……..…….

3.2 Mechanical testing and modelling ……..……..……

3.2.1 Indentation ……..……..

3.2.2 Bending ……..……..……..……..

3.2.3 FE modelling ……..……..

In this work it was produced a biocompatible and nanostructured calcium phosphate coating on pure titanium with the variation of the synthesis time and the in the presence/absence of a titanium oxide layer. Then the mechanical properties of pure titanium and coated titanium were evaluated. It is recommended that the hydrothermal method be carried out a high temperature since the dissociation constants of the calcium–citrate complexes mentioned before increase with temperature. It is understood that heating up the solution promotes complex dissociation and subsequent release of calcium ions, which become available for the nucleation and growth of the hydroxyapatite particles. In addition to this, heating the solution also contributes to supersaturation, as hydroxyapatite solubility decreases with temperature increase [26].

3.1. Physical-chemical characterization

3.1.1. Effect of the presence of titanium oxide layer on coating morphology

The SEM images of calcium phosphate coatings on pure titanium produced in the absence and presence of titanium oxide layer after 6 hours in hydrothermal conditions are shown in figure 3.1a, b and 3.1c, d respectively. It is observed that the surface without oxide layer it is completely covered with small particles with a rod like shape. For the samples with oxide layer, it is possible to observe that there is a continuous and uniform calcium phosphate layer and the formation of agglomerated CaP nanoparticles with needle like shape, on top of the calcium phosphate layer (figure 3.1b). It is also observed the presence of defects on surface (polishing defects) in all titanium coated samples. Doing a comparative analysis of the obtained morphologies in absence and presence of titanium oxide layer, it is observed that the presence of oxide induces the formation of small nanoparticles on Ti subtract, while in the absence of oxide layer it is observed agglomeration of big particles with needle shape. In all cases it isseen a total coverage of the titanium surface.

Figure 3.1.1 shows the SEM images, and it reports the morphology of treated Ti samples, showing the coating and chemical components present in the coating:

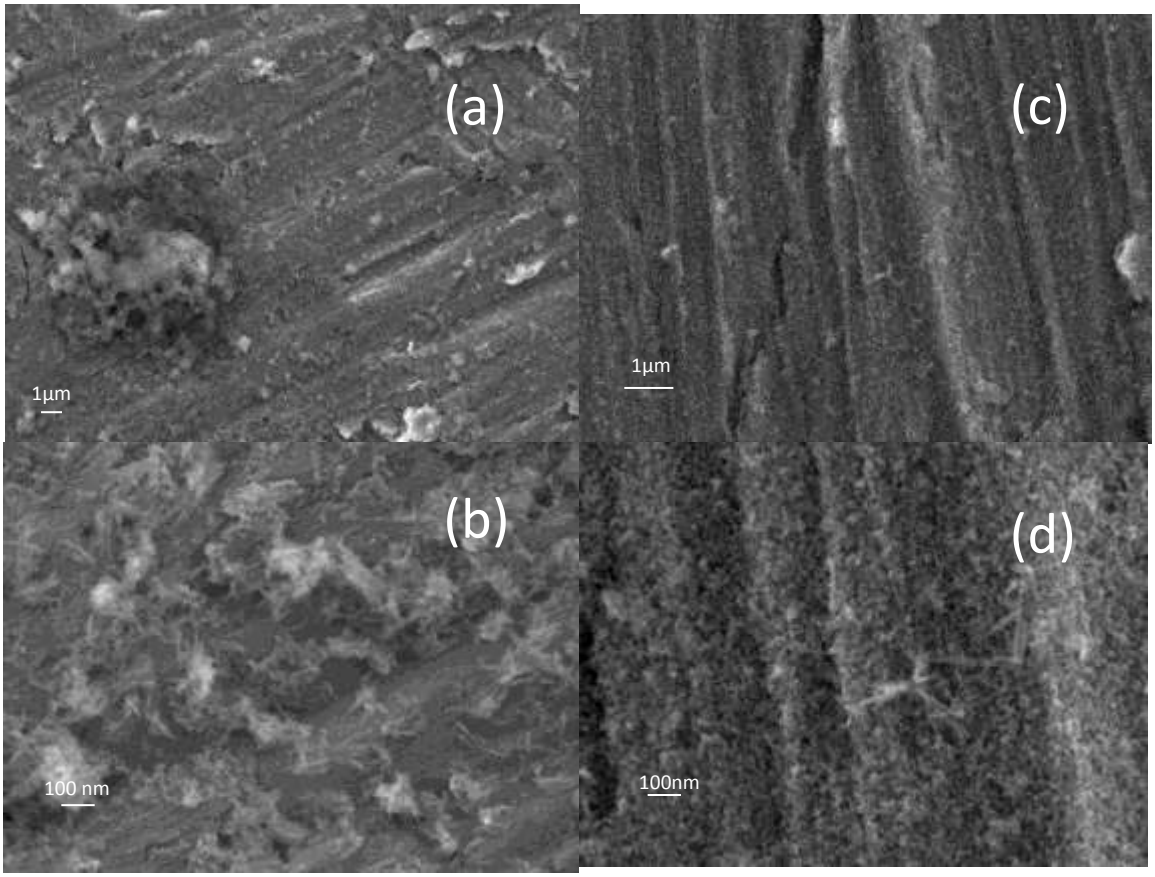

Fig 3.1.1.. SEM images of the calcium phosphate coating synthesized after 6 hours in (a, b) (Ti6NO) absence of titanium oxide layer, (c, d) (Ti6O) in presence of titanium oxide layer

The presence of cracks in the oxide layer is reported inreference [27] and it could be assumed an improvement,in that our oxide layer is uniform and without apparent cracking.

The surface of the produced coatings was also evaluated by AFM as represented in figure 3.1.2 and 3.1.3. The rod-like morphology observed in SEM pictures from the calcium phosphate coating produced without oxide is confirmed by AFM. The nanostructures have a width of ~100 nm and a length of 150 nm (figure 3.1.2b).

The size and the morphology of the calcium phosphate nanostructures formed on titanium with oxide layer are more difficult to evaluate by AFM, however they seem tohave a size less than 100 nm and a round like shape (figure 3.1.2c).

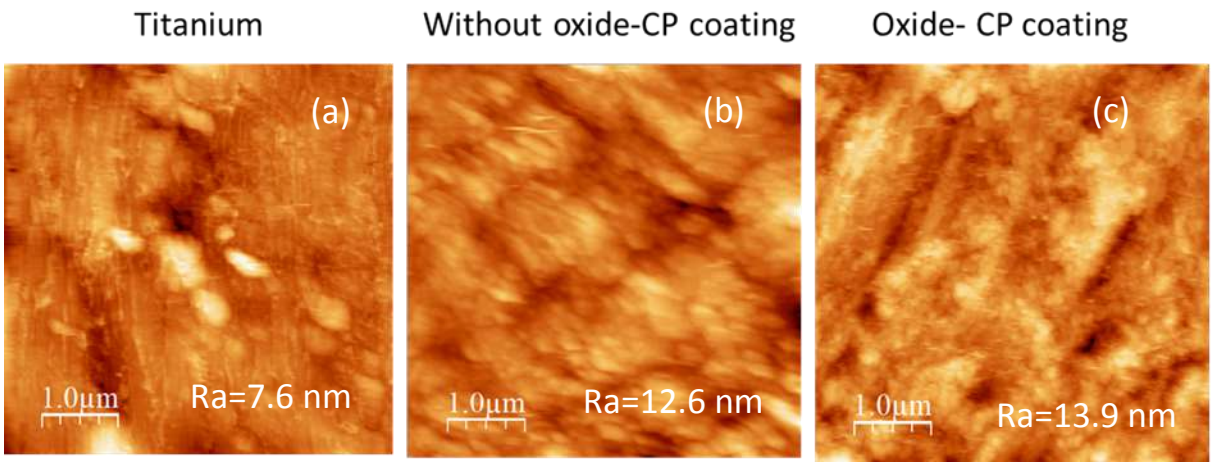

Fig 3.1.2. AFM pictures at 1µm of titanium and titanium coated with calcium phosphate in presence and absence of oxide layer at 6 hours by hydrothermal treatment

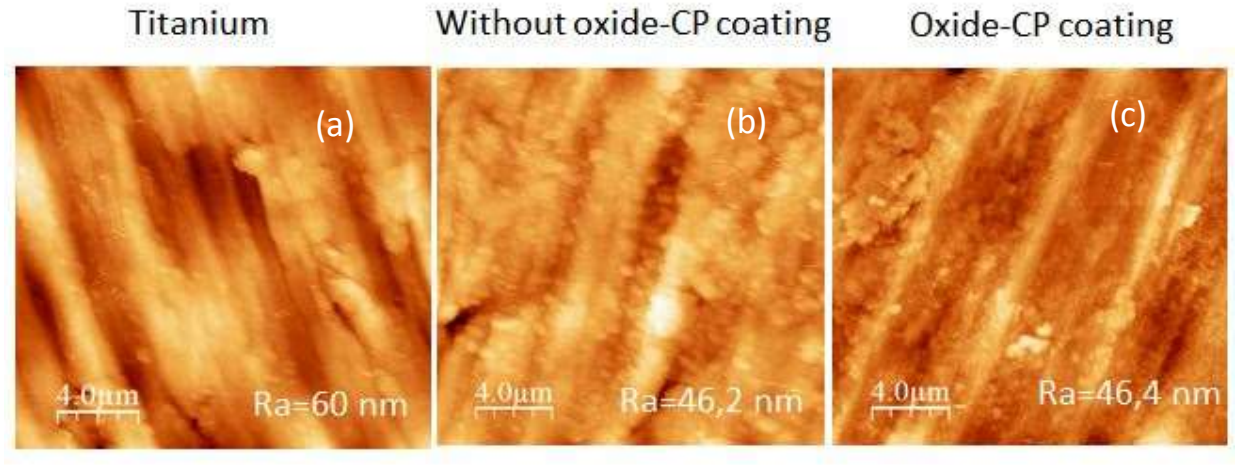

Fig 3.1.3. AFM pictures of at 4 µm titanium and titanium coated with calcium phosphate in presence and absence of oxide layer at 6 hours by hydrothermal treatment

The roughness of titanium oxide layer defined in the literature [27] is $R_a = 10nm$. As it can be seen in figure 3.1.2, our value of roughness in coating with oxide layer is in the same order of the magnitude. Comparing the roughness between calcium phosphate coating without oxide and with oxide, at low magnification the values are 12,6 nm and 13,9 nm, varying only slightly and they are in the same range of magnitude. At high magnification the results remain in the same value of 46 nm. Having a nanocoating with a low roughness, the biocompatibility of the coated implant will be better to biomedical applications [27].

Then it can be observed (figure 3.1.2 and 3.1.3) that the presence of oxide layer does not have influence in the roughness of the calcium phosphate coating.

To characterize the chemical composition of the formed calcium phosphate coating on the Ti substrate mentioned above, EDS analyses were performed as well as EDX maps. In figure 3.1.4a and b the EDS analyses of both coatings produced after 6 hours (without (3.1.4a) and with oxide (3.1.4b)) is

presented. It is observed that the elements that are present in both coatings for this resolution are calcium (Ca), phosphorus (P) and oxygen (O). Using the EDS results it was possible to estimate the Ca/P ratio. The obtained Ca/P ratios were 1.42 for coatings without oxide and 1.23 with oxide. These values are lower than the Ca/P ratio of stoichiometric hydroxyapatite (Ca/P-1.67) [28]. The obtained result suggest that coatings are nonstoichiometric, which occurs when the apatite contains HPO_2^{4-} ions in place of PO_3^{4-} ions or when carboxylate (C) replaces phosphate groups (P) [28]. In this last case, the Ca/P ratio should be considered as Ca/(P+C). It was impossible to determine the amount of carbon since all samples were coated with a uniform carbon film to do SEM pictures.

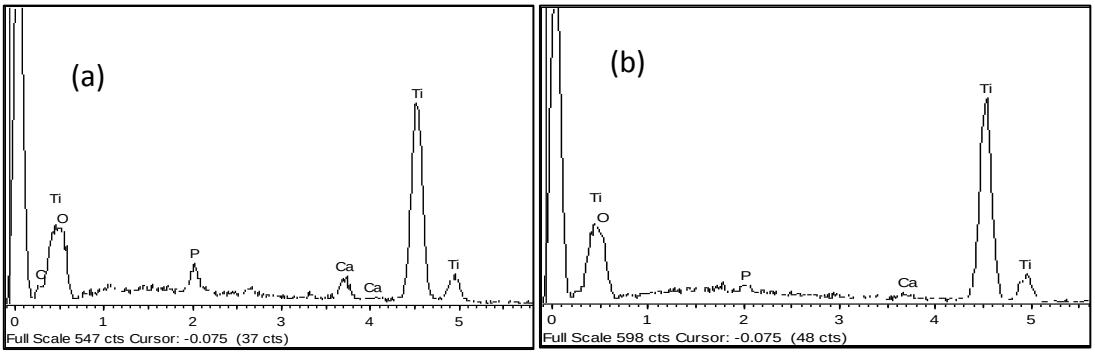

Fig 3.1.4. EDS analysis of calcium phosphate coating on pure titanium at 6 hours (a) without oxide layer, (b) with oxide layer.

In figure 3.1.5 (a, b, c and d) it is observed the elements distribution (EDX maps) that constitute the coating, namely: oxygen (O), calcium (Ca) and phosphorus (P). Also is also presented the EDX maps for the substrate titanium. These results also allowed a qualitative analysis of the coating thickness. It was observed that the thickness of both coatings is less than 10 μm, since the titanium (Ti) signal is detected in the EDX maps. The Ca and P signal present in all surface confirms the formation of a calcium phosphate on top of titanium. In the presence of oxide layer the Ca and P signal is more intense in nanoparticles agglomerates (figure 3.1.5 e and f) when compared with titanium signal, which is less intense in these agglomerates.

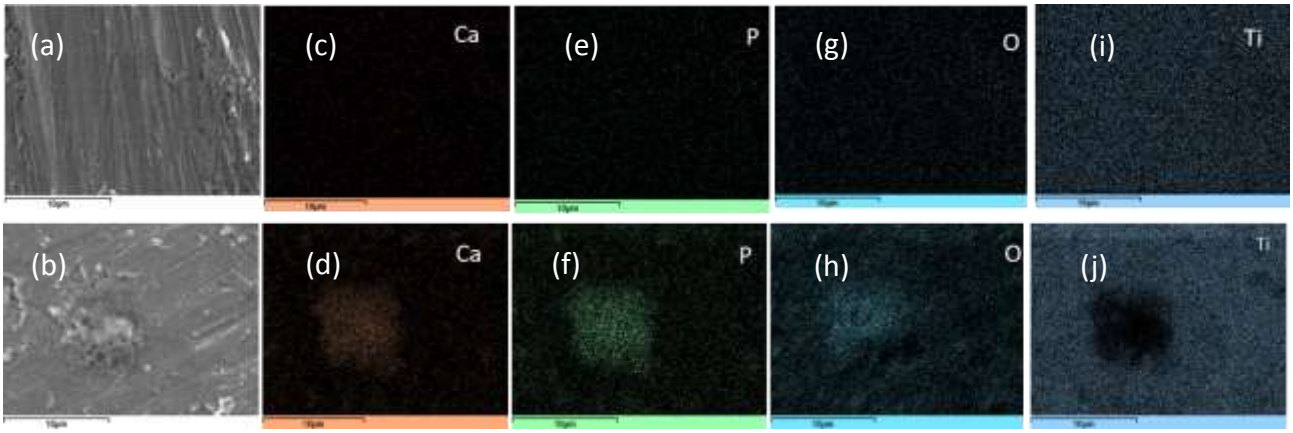

Fig 3.1.5. SEM picture of calcium phosphate coating (a) without and (b) with oxide layer; EDX maps of calcium, phosphorus, oxygen and titanium elements respectively (c, d; e, f; g, h; i, j).

In order to evaluate the chemical composition of the obtained coatings the ATR- FTIR technique was applied. In ATR-FTIR technique, each sample has been tested with attenuate total reflection (ATR) and the results obtained are presented in figure 3.1.6, 3.1.7 and 3.1.8.

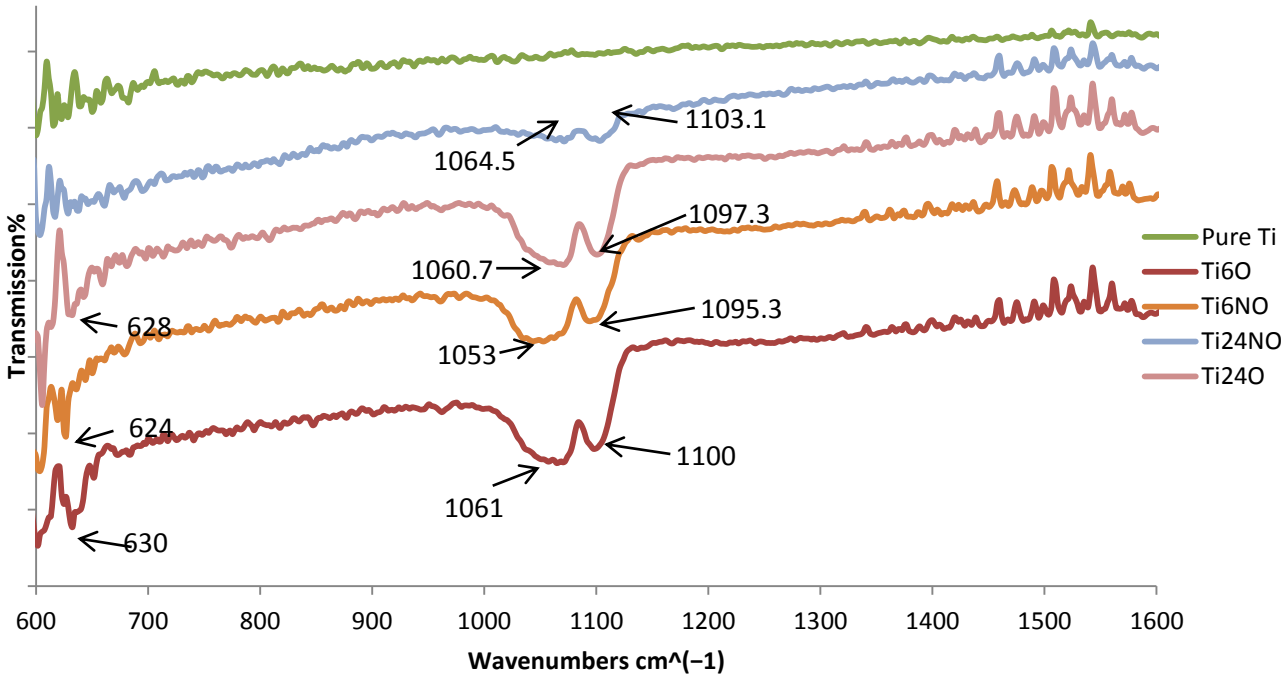

Fig 3.1.6. FTIR results corresponding to pure titanium and HAp coating obtained by hydrothermal process: magnification of the 600-1600 cm^{-1} spectral region.

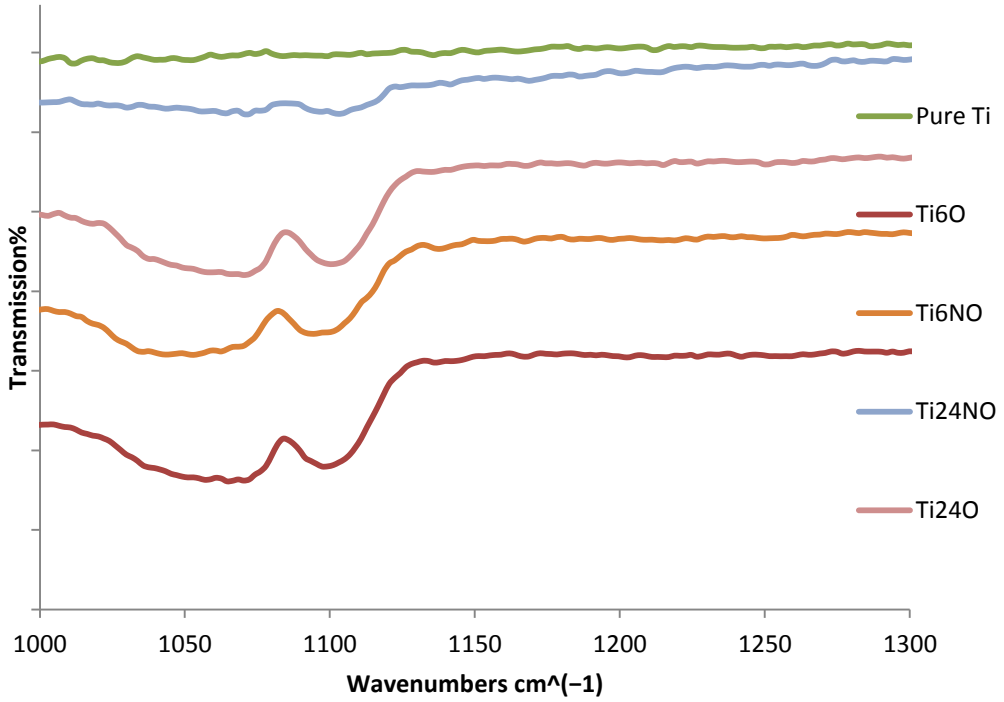

Fig 3.1.7. FTIR results corresponding to pure titanium and HAp coating obtained by hydrothermal process: magnification of the 1000-1300 cm^{-1} spectral region.

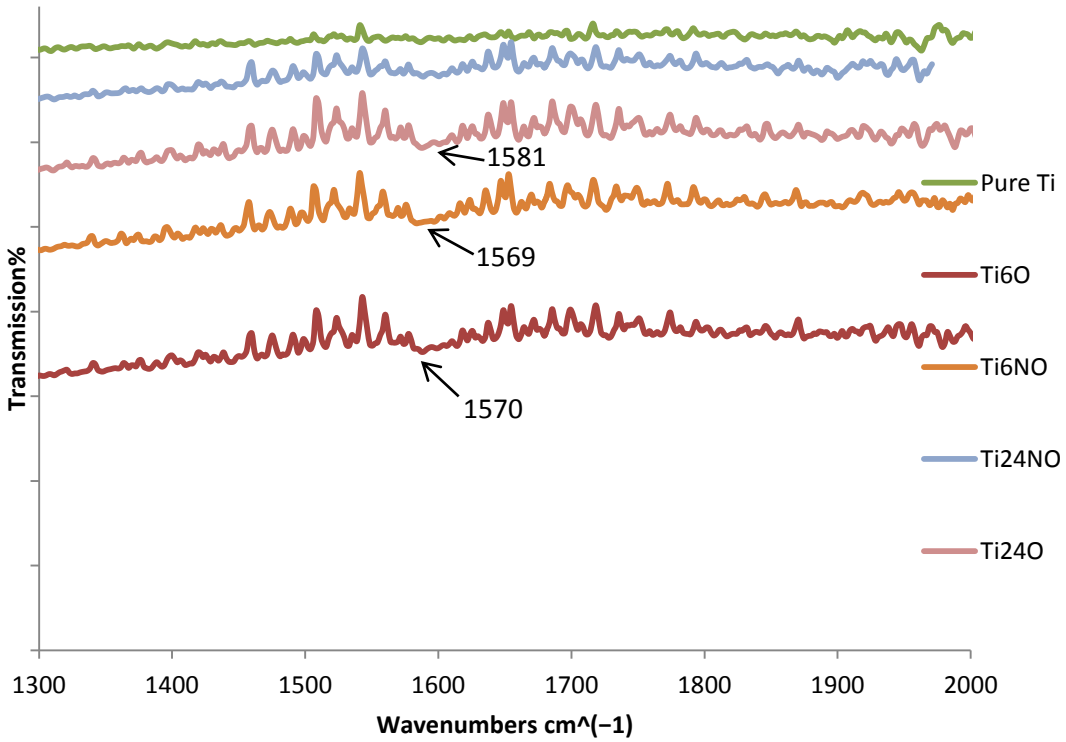

Fig 3.1.8. FTIR results corresponding to pure titanium and HAp coating obtained by hydrothermal process: magnification of the 1300-2000 cm^{-1} spectral region

In figure 3.1.6 it is observed a well-defined band at 1100 cm^{-1}, characteristic of hydroxyapatite. Additionally it is identified three different vibrations: The first peak, at 1092 cm^{-1}, arises from a triple degenerate antisymmetric stretching mode vibration, of the PO_4^{3-} groups υ3. The other vibration band of this degenerate vibration, υ3, of the P-O bond appears at 1052cm^{-1}. The peak at 962 cm^{-1} is characteristic bands of PO_4^{3-} ions (υ1 band). The shift in the obtained peaks is indicative of an modification of the ions in the vicinity of the phosphate groups. As Ca/P ratio is lower than 1.667, there is no crystalline HAp coating, and the presence of the group P+Cit could be present in the coating.

The peaks at 602cm^{-1}, 605 cm^{-1} and 601 cm^{-1} are present in all coating samples and they correspond to PO_4^{3-} υ4 [28]. In addition the peaks at 584 cm^{-1} and 594 cm^{-1} define the same group (PO_4^{3-}). It can be seen that in Ti6O and Ti24O they are better defined, followed by Ti6NO. There are no presences of these peaks in Ti24NO, which suggest that the presence of PO_4^{3-} is very low.

The figure 3.1.8 shows a peak at 1570 cm^{-1}, which is typically of carboxylic groups from citrate ions [28]. Then it can be justified the Ca/P ratio lower than 1.667 with the presence of the group P+Cit, that is a big presence of carbon is detected. This peak is also well-defined in presence of oxide layer (figure 3.1.8).

In order to compare the influence of the oxide layer in ATR-FTIR results, it can be seen that Ti6O has the characteristic peaks of hydroxyapatite better defined than Ti6NO. This suggests that the presence of the oxide layer is important for coating formation.

The crystal structure of the coating was also analysed by XRD. Figure 3.1.9 presents the XRD diffraction patterns of titanium, titanium coated with calcium phosphate after 6 hours with and without oxide layer in 2θ range of 20°–60°. As observed the only crystalline phases that are detected in XRD patterns are titanium and anatase phase. These peaks observed are from titanium substrate, which suggest that it was produced a nanometric-thick calcium phosphate coating. From the XRD results it was not possible to identify and characterize the calcium phosphate phase formed on titanium.

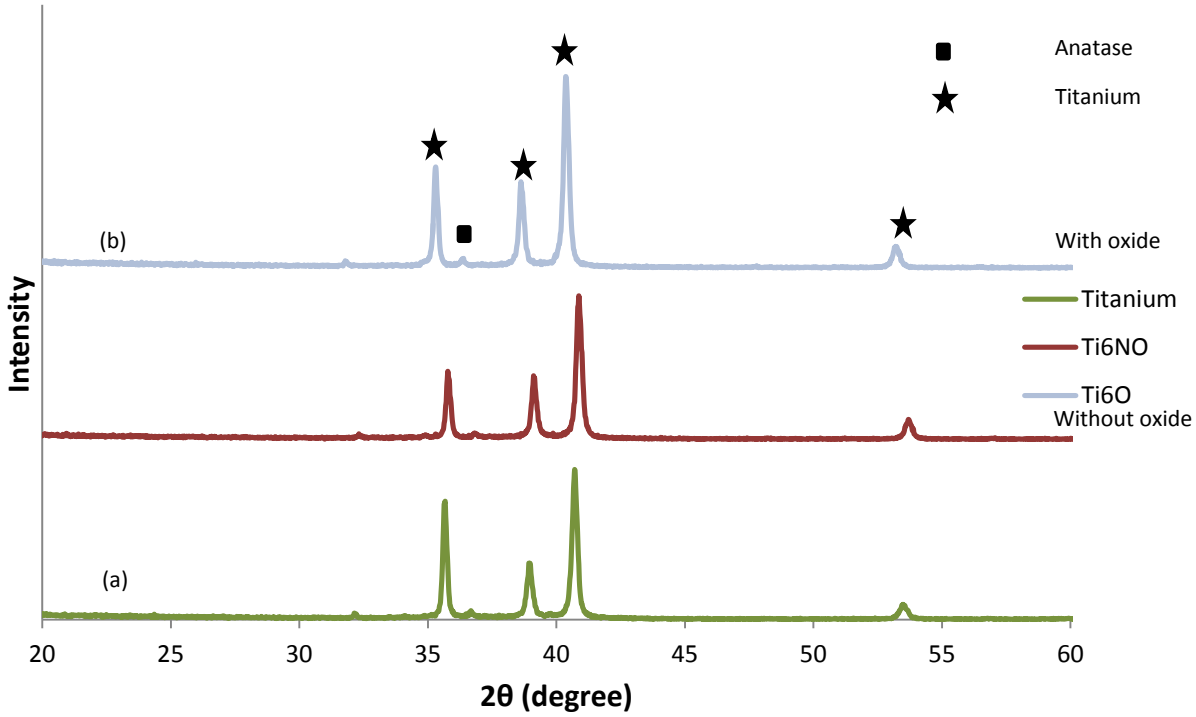

Fig 3.1.9. XRD patterns of (a) pure titanium, (b) calcium phosphate synthesized on titanium with and without oxide layer

In figure 3.1.10, a magnification of XRD patterns is presented in order to analyze the characteristic hydroxyapatite range from 25° to 45°.

The XRD patterns of all samples are mostly similar and no characteristic diffraction peaks of CP phase could be detected. Only there is a small peak at 2θ=32 ° which should be higher to be identified, as HAp is present in the coating, because it might be assigned to the presence of minor amounts of pure crystalline calcium phosphate phase [26]. This is due to the particle size of the coating being in the order of nanometers, so there is no difference in the X-Ray results.

With these results, it is only possible to identify different forms of crystals (anatase structure). Regarding to the literature, anatase crystals come out on the surface of titanium from inside after hydrothermal treatment for 6 hrs. Therefore, mixed-structure is formed as HAp and anatase after hydrothermal treatment for 24 hrs. Due to this, the anatase can be identified in the results and it is predominant.

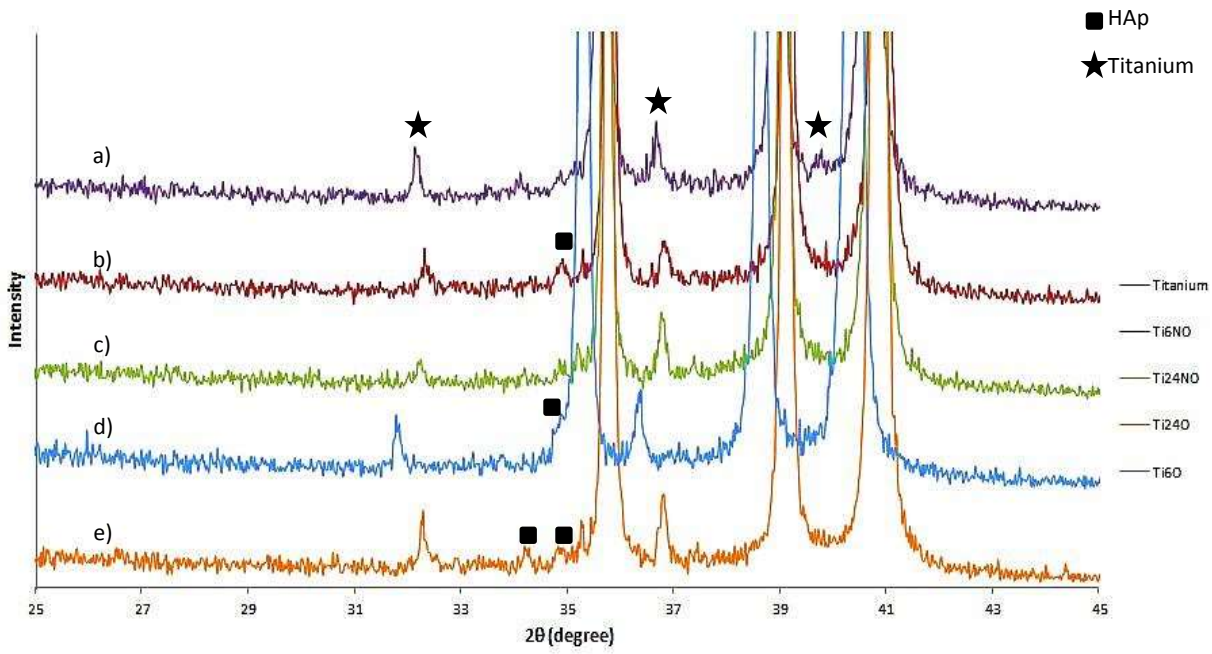

Fig 3.1.10. XRD patterns from 25º to 45º of (a) pure titanium, (b) CP synthesized in 6 h on Ti without oxide, (c) CP synthesized in 24 h on Ti without oxide layer, (d) CP synthesized in 6 h on Ti with oxide and (e) CP synthesized in 24 h on Ti with oxide layer

The XRD patterns in figure 3.1.10 show the diffraction peaks in all the cases. Making a magnification in peaks at 34º and 35ºm thiscould be probably recognized as deposition of the thin HAp layer. In Ti6NO and Ti6O it is identified a small peak at 35º, as these peaks are characteristic from HAp coating [4]. Assuming that the peak in Ti6O is superimposed to the higher characteristic peak of titanium at 35º, it could be said that in presence of oxide layer, the peak has a better definition than in absence of oxide layer. However, assuming the big magnification, it cannot be affirmed the presence of the HAp coating.

A fracture of the sample was performed in order to observe the thickness of the coating. As it can be seen in figure 3.1.11, the coating is uniform and has a thickness of the order of 100 nm. The coating's thickness was thoroughly characterized using broken sections shown in figure 3.1.11. The thicknesses were assessed directly from SEM images at 100 µm for Ti substrate.

These images show the thickness in the presence of titanium oxide (figure 3.1.12) and without it (figure 3.1.11). It can be seen that in the absence of oxide layer, the coating has a smaller particle size and without agglomerations. In both cases, the coating is uniform but in presence of oxide layer the coating is well-distributed.

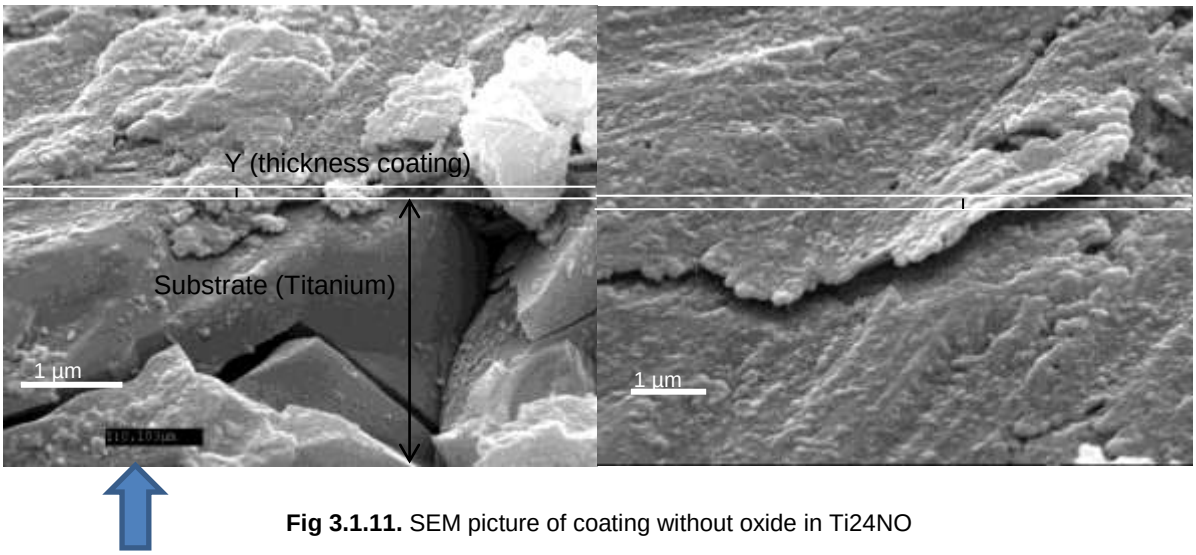

Fig 3.1.11. SEM picture of coating without oxide in Ti24NO

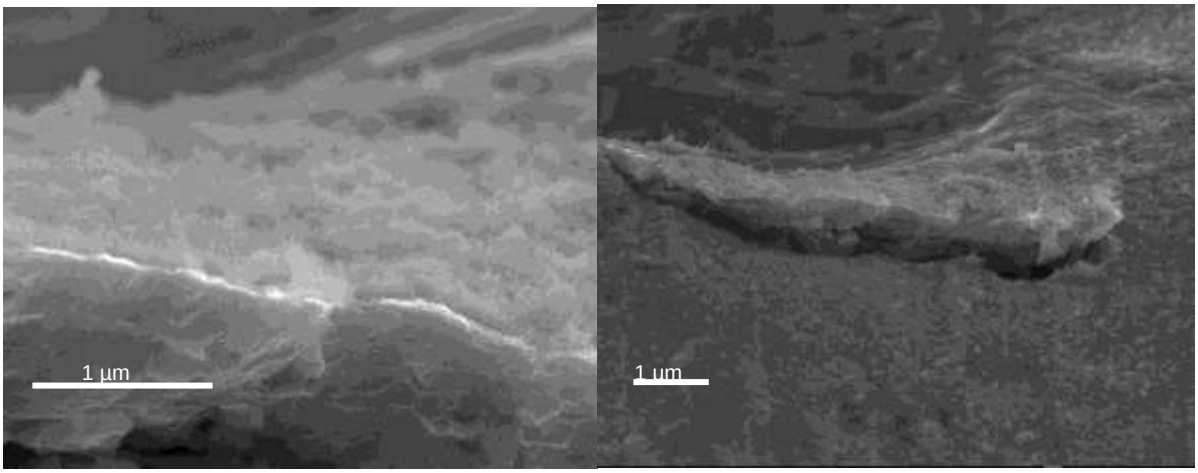

Fig 3.1.12. SEM picture of coating with oxide in Ti6O

The figure 3.1.13 shows the contact angle by measuring the wettability of the coating in presence of oxide and in absence of it:

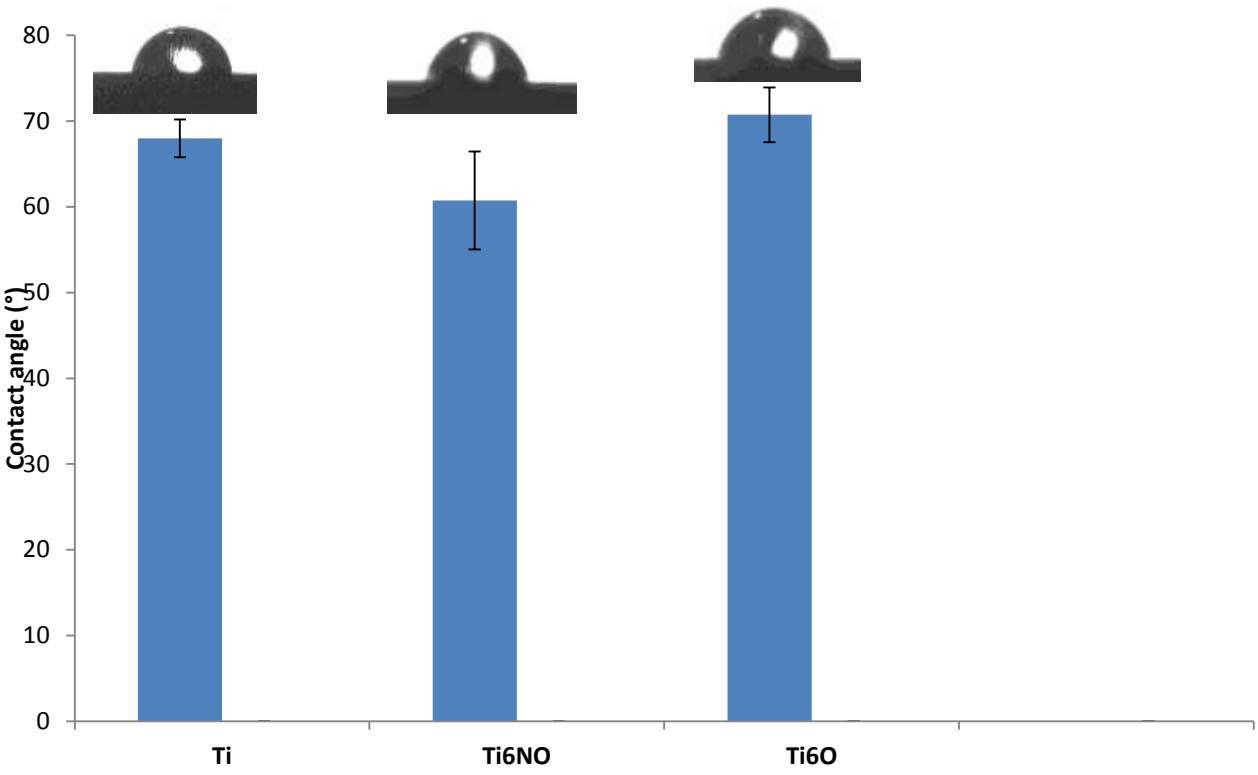

Fig 3.1.13. Static contact angle measurements on pure titanium and HAp coatings in plane samples

A value of 82° of contact angle is assigned to commercial pure titanium [2]. As it can see, 68° has been obtained for this test. This value is a bit lower and it could be attributed to the influence of the presence of the titanium oxide layer.

Regarding to the coating, the absence of oxide layer improves the wettability of the coating, making the surface moderately more hydrophilic. When oxide is present, the difference is not very significant comparing with pure titanium.

3.1.2. Effect of the synthesis time

The SEM images of calcium phosphate coatings on pure titanium produced at 24 hours in absence and presence of titanium oxide layer in hydrothermal conditions are shown in figure 3.1.14a, 3.1.14b and 3.1.14c, 3.1.14d respectively. It is observed that the surface, when the coating is produced in 24 hours and with oxide layer, has an uniform coating with very small particles and well distributed. However, when the coating is deposited without oxide, there is a low quantity of CP and the coating is not as uniform.

Figure 3.1.14 shows the SEM images, and it reports the morphology of treated Ti samples, showing the coating and its distribution:

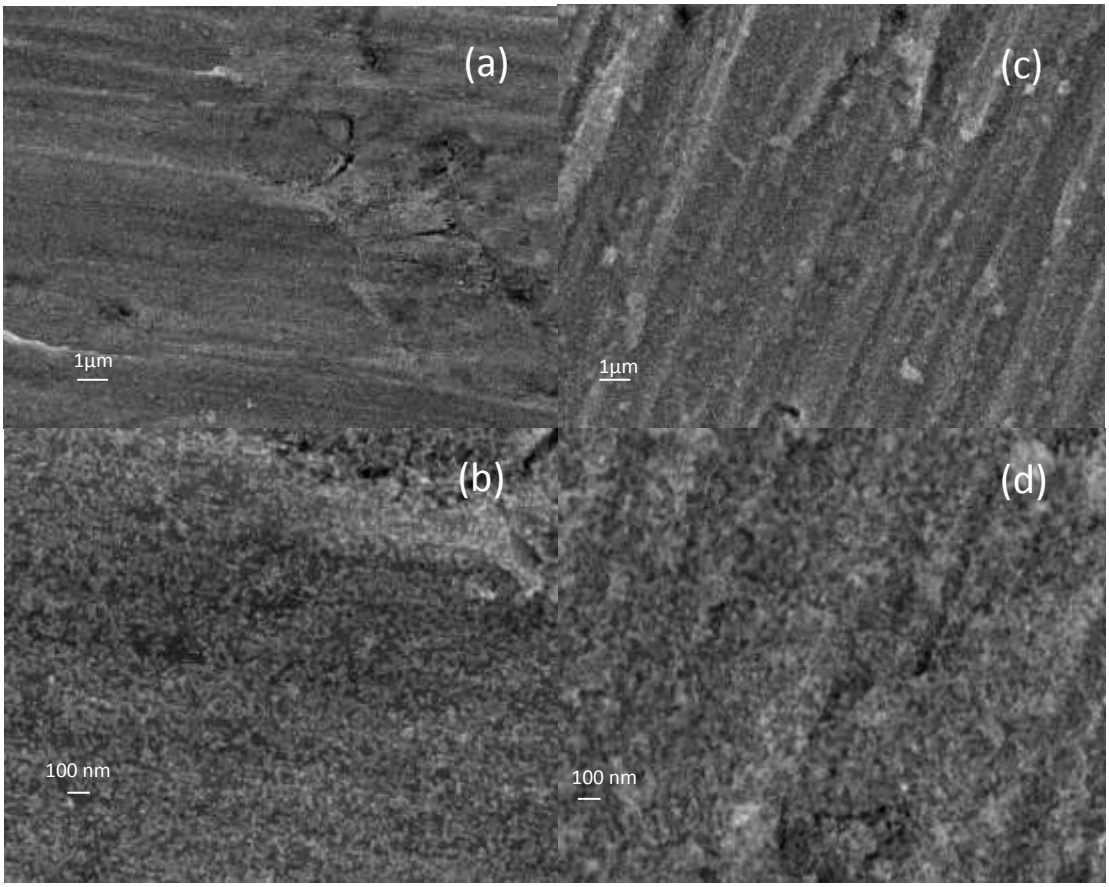

Fig 3.1.14. SEM images of the calcium phosphate coating synthesized after 24 hours and without oxide layer (a, b) (Ti24NO) and in presence of titanium oxide layer (c, d) (Ti24O)

Comparing SEM images at 24 hours from figure 3.1.14 with the figure 3.1.1 at 6 hours, it can be concluded that at 24 hours the coating is more uniform due to the presence of the agglomerations at 6 hours. In addition, a small particle size is observed in 24 hours.

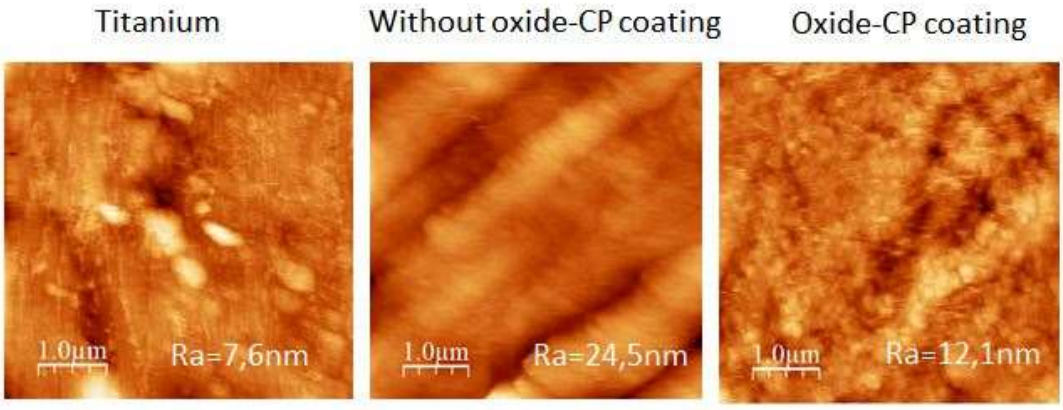

Fig 3.1.15. AFM pictures at 1µm of titanium and titanium coated with calcium phosphate in presence and absence of oxide layer at 24 hours by hydrothermal treatment

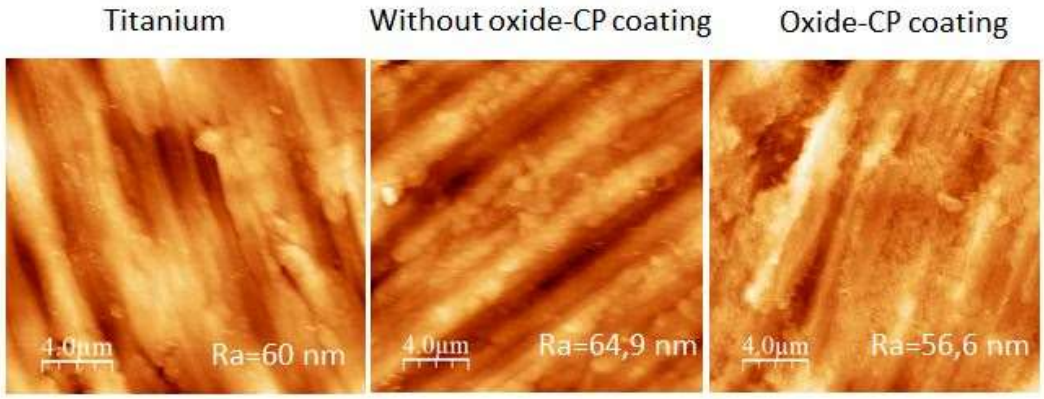

Fig 3.1.16. AFM pictures at 4 µm of titanium and titanium coated with calcium phosphate in presence and absence of oxide layer at 24 hours by hydrothermal treatment

Regarding to the results, the surface of pure titanium in presence of oxide layer shows a small roughness on the nanoscale with a value of R_a= 7,6 nm.

As it can be seen in figure 3.1.15, the specimen without oxide layer exhibits higher surface roughness (R_a=24,5 nm), as R_a is the double of the value compared to the sample in presence of oxide (R_a=12,1 nm). In figure 3.1.2 at 6 hours, there was no difference between the values (R_a=12-13 nm), but in this figure there is a big change in the presence of oxide. Then, a longer time and in absence of oxide layer, a higher roughness of the coating is obtained. Besides that, the roughness increases when the hydrothermal time is higher, since at 6 hours at high magnification the roughness got is R_a=46 nm and at 24 hours it varies from R_a=65 nm to R_a=57 nm.

On the other hand, due to the low thickness of the coating, the values obtained do not differ too much from the roughness of pure titanium.

Regarding to the bibliography, coatings have good results regarding to the roughness. The relevance of the presence of a nanotextured layer is here discussed: surface nanotopography can be used to selectively modulate the response of osteoblasts and bacteria, because their size and rigidity are

different. Nanoscale surface patterns and roughness can attract osteoblasts, through specific integrin recruitment and the response of filopodia and lamellipodia. On the other side, while a surface with roughness on the micro scale (0.5 μm or higher) can induce a higher bacterial proliferation, the selection of a roughness on the nanoscale can be useful to reduce bacteria adhesion, when it is required [27].

The roughness of the coating in TI24NO increases comparing with pure titanium while the others lower it. Therefore the coating in TI24NO has higher HAp particle size, followed by TI6O, TI6NO and finally TI24O which seems the thinnest. Comparing with the results of contact angle, it could be said that the thinner coating is obtained, and lower contact angle.

Table 5. Summary of roughness

Sample	Ra (nm) (at 1μm)	Ra (nm) (at 4μm)
Pure titanium	7,6	60,0
TI6NO	12,6	46,2
TI24NO	24,5	64,9
TI6O	13,9	46,4
TI24O	12,1	56,6

Then it is presented in figure 3.1.17 the EDS spectrum for the treatment in 24 hours. It can be assumed that the quantity of Ca/P is lower than in 6 hours, but the coating is more uniform and with a smaller particle size.

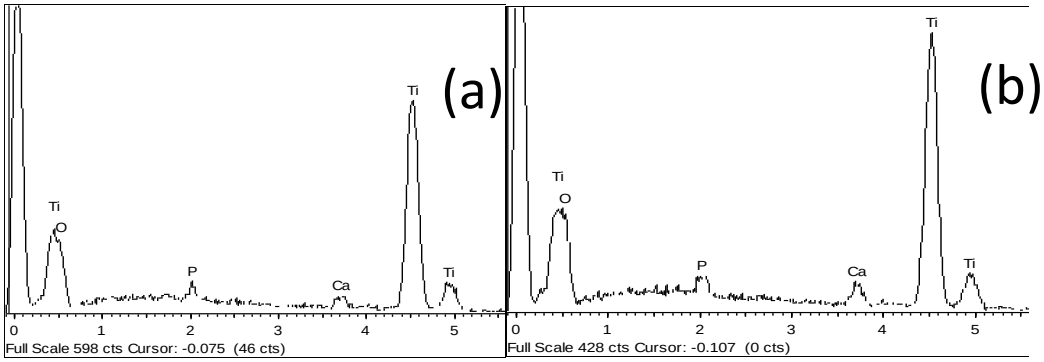

Fig 3.1.17. EDS analysis of calcium phosphate coating on pure titanium at 24 hours (a) without oxide layer, (b) with oxide layer.

In figure 3.1.18 (a, b, c and d) it is observed the EDX maps for the several elements that constitute the coating, namely: titanium, oxygen, calcium and phosphorus. The Ca and P signal present in all surface confirms the formation of a calcium phosphate on top of titanium.

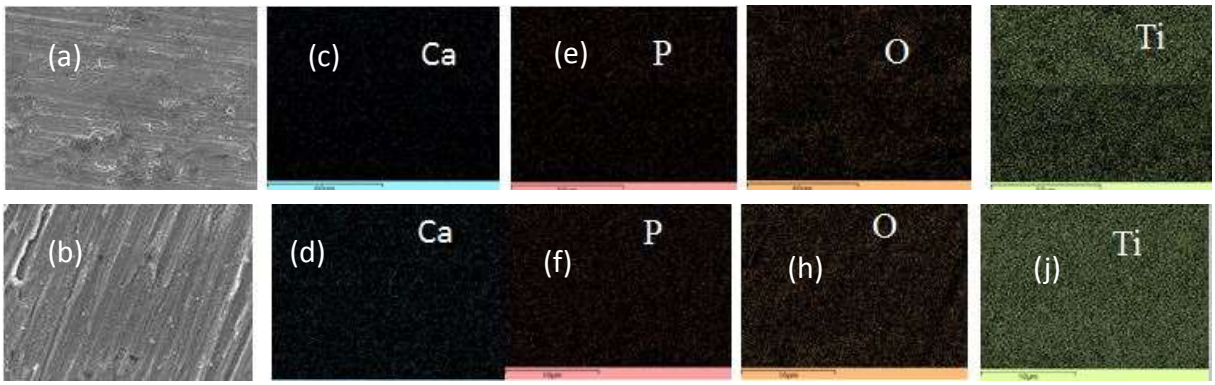

Fig 3.1.18. SEM picture of calcium phosphate coating at 24 hours (a) without and (b) with oxide layer; EDX maps of calcium, phosphorus, oxygen and titanium elements respectively (c, d; e, f; g, h; i, j).

In ATR-FTIR technique, as it said before in figure 3.1.6, peaks at 1100 cm^{-1} are typically from HAp. The peaks 566 and 602 cm^{-1} are assigned to a doubly degenerate bending mode (υ4 band PO_4^{3-} groups). On the other hand, the band at 632 $\mathrm{cm}^{-1}$is originated from OH^- group [8, 26].

Regarding to the ATR-FTIR results, Ti6O, and Ti24O have well-defined peaks as for the presence of the HAp layer due to the peaks are well defined at 1060 $\mathrm{cm}^{-1}$and 1100 cm^{-1}. Then TI6O has a lower definition and finally Ti24NO, in which it's difficult to appreciate PO_4^{3-} ions and the band at 1064 it is not defined. In addition, it can be seen that when the coating is formed in presence of oxide layer the HAp peaks are very similar and well defined.

Comparing both calcium phosphate coatings synthesized for 24 hours, it can be seen a difference in the bands as mentioned before, with the phosphate groups more evident in the coating produced on top of titanium with oxide layer (Ti24O).

In the range of 632 cm^{-1} to 642 cm^{-1}, the peak for OH for hydroxyapatite is defined and it suggests the interaction of TiO_2 layer and HAp coating [2]. Then this peak is well defined for both conditions, with and without oxide layer. However, when the time increases, this interaction disappears, so that there is lower interaction between both layers and it's better in presence of the oxide layer, since the peak is a bit defined.

Regarding to XRD patterns in figure 3.1.10, in Ti24O is possible to identify two smalls peaks in the range of 35º, and comparing with Ti24NO, no peak is detected when coating is in absence of the oxide layer. On the other hand, Ti24O has a better definition on these peaks comparing with Ti6O, however they are very small in all the cases and due to their definition it cannot be affirmed the presence of the HAp coating.

Considering that surface roughness and topography highly affect surface wettability, the wettability of the polished and coating surfaces was evaluated. The figure 3.1.19 shows contact angles for all the samples:

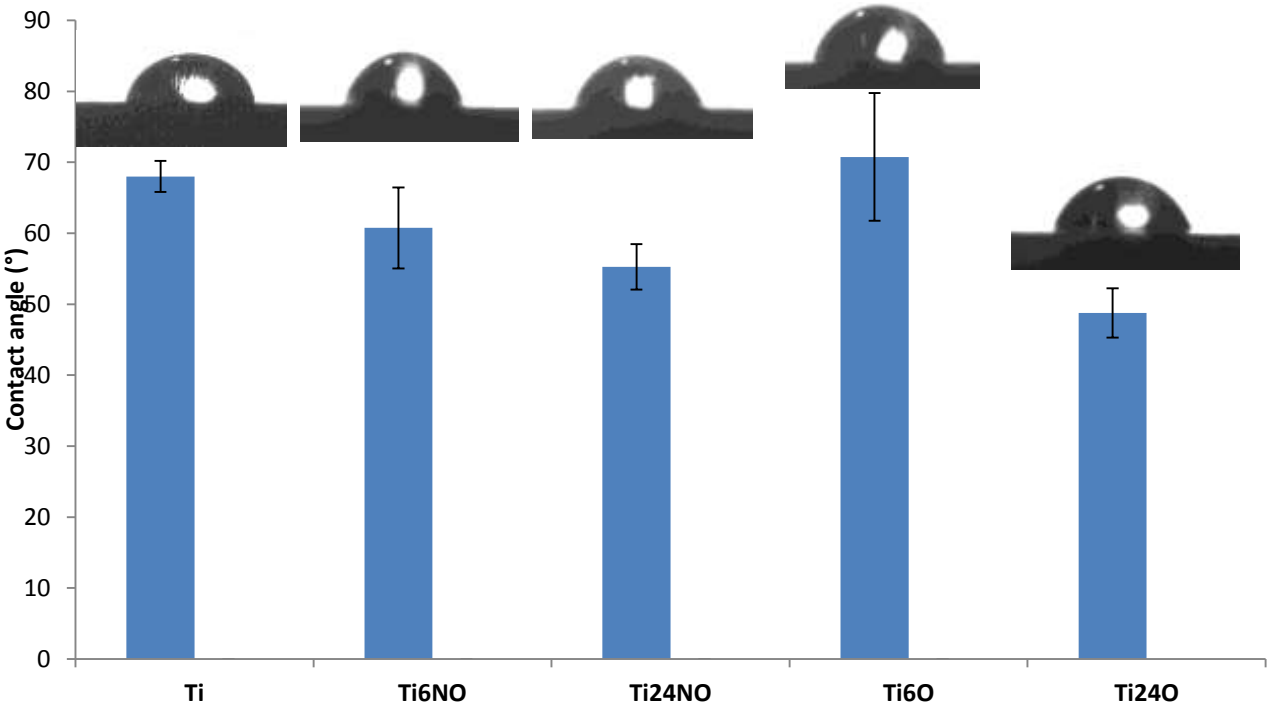

Fig 3.1.19. Static contact angle measurements on pure titanium and HAp coatings in plane samples

As it can be seen in figure 3.1.19, the contact angle in Ti6NO, Ti24NO and Ti24O is reduced in comparison with pure titanium. However, contact angle in Ti6O is higher and this is due to one of the drops having an angle higher than 90°. Then an increase in the surface wettability has been observed for the samples Ti6NO, Ti24NO and Ti24O, being the Ti24O the best result because has the lowest contact angle between the surface and the drop. Then as it can be observed in the figure, the contact angle in coatings obtained in 24 hours is reduced more than in 6 hours, confirming an increase of the wettability at 24 hours.

It's interesting this result, considering that high wettability of the implant by the physiological fluid is believed to facilitate protein adsorption, formation and cell attachment [27]. Then, it is observed that with a higher coating time, the contact angle decreases. From this section, it can be assumed that the presence of TiO_2 doesn't have influence when the hydrothermal treatment is made during 6 hours but there is influence in 24 hours.

The wettability data correlate well with the surface roughness findings. Analyzing the results, when the time is 6 hours in presence of oxide layer the roughness is $R_a = 13\text{nm}$ and the contact angle value is 70º, and without oxide layer is $R_a = 13\text{nm}$ and the contact angle is 62º. On the other hand, analyzing the results at 24 hours, in presence of oxide layer the roughness is $R_a = 56\text{nm}$ and the contact angle is about 55º, and in absence of oxide layer the roughness is $R_a = 65\text{nm}$ and the contact angle is 49º. Comparing all results, it is observed that a worst adhesion of the coating is obtained in 6 hours due to high contact angle value obtained, which corresponds to the low roughness value. However, when the time to perform the coating is 24 hours, the roughness is higher and the contact angle is reduced. Then the wettability increase in the case of 24 hours and in presence of oxide layer.

3.1.3. Summary

In order to compare the results, a summary of the results in all the tests is presented in the following table:

Table 6. Summary of all the results

	6 hours	24 hours
Presence of TiO_2	- Agglomerations - Contact angle of 70° - Large band at 1060 cm^{-1} - Ra=13.9 nm	- Small particle size - Contact angle of 49° - Large band at 1060 cm^{-1} - Ra=12.1 nm
Non presence of TiO_2	- Uniform coating - Contact angle of 62° - Normal band at 1060 cm^{-1} - Ra=12.6 nm	- Big particle size - Contact angle of 55° - Loosing band at 1064 cm^{-1} - Ra=24.5 nm

Table 7. Summary of values of relevant results

Sample	Ra (nm) (at 1µm)	Contact angle	Berkovich Hardness	Young's Modulus(E)
Pure titanium	7,6	68	29,51	102
TI6NO	12,6	60,75	30,41	31,20
TI24NO	24,5	55,25	27,55	43,46
TI6O	13,9	70,75	13,96	30,87
TI24O	12,1	48,75	24,90	40,04

As it can be seen, TI24NO has the highest roughness, so that, it has the highest particle size and the roughness in TI24NO increases comparing with pure titanium while in the others decrease. In addition, a reduced value of contact angle in this sample is obtained and it means that the wettability of the surface has been increased. .

On the other hand, TI6NO has a low roughness, which means that the size of the particles is very small. The contact angle in this sample is reduced in comparison with pure titanium, so the wettability has increased a little bit. Young's modulus is lower and hardness is very similar to pure titanium.

Regarding to TI6O, the roughness is intermediate. However the contact angle is higher, so that, the wettability and, therefore, the adhesion decreases in this coating. Young's modulus in this sample is lower than in pure titanium and it has the lowest value of hardness.

Finally, the coating in TI24O seems the thinnest due to the lowest value or roughness and, therefore, this coating has the lowest particle size. Moreover, it has the lowest contact angle value, so that, it has the best adhesion. Although the hardness is lower than pure titanium, Young's modulus is not as low as in the 6 hours cases.

3.2. Mechanical testing and modelling

3.2.1. Indentation

The stress-shielding effect is aphenomenon related to implant failure. In the case of orthopedic implants, the bone is not properly loaded, because of implant rigidity and, consequently, the implant is progressively loosened, due to bone atrophy. In particular, the Young's modulus value for the bone ranges between 6.9±4.3 GPa and 25.0±4.3 GPa, while the same value for Cp-Ti is 103–107 GPa [18]. It seems that this situation is inhibited or at least decelerated with the use of more complacent implant materials.

On the other hand, the hardness of thin hydroxyapatite coating has been studied using the nanoindentation method. The hardness of the nanocrystalline HAp coating is close to the hardness of the HAp single crystal (about 10 GPa) and it corresponds to the average hardness of hydroxyapatite single crystals. This fact can be explained as follows. At the initial stage of the deformation, there occurs a lightweight sliding along the grain boundaries. It is limited by triple grain junctions and kinks on flat fragments of the boundaries. The deformation produced by this sliding can amount to 0.01–0.10 fraction of the total elastic deformation. This follows from the calculations of the elastic modulus of polycrystals and from the experimental data on the height of the grain boundary internal friction peak and indicates a small contribution of the grain boundary sliding to the total plastic strain. Nonetheless, the presence of a weak link in the plastic deformation in the form of grain boundaries leads to a concentration of mechanical stresses at obstacles (triple junctions) for sliding along the grain boundaries, which contribute to the destruction of the HAp crystal structure[29].

The decrease in the hardness of HAp in the amorphous state is explained by the decrease in the number of chemical bonds between the contacting atomic clusters. The plastic deformation of HAp in the crystalline and amorphous states occurs according to the same mechanism—the breaking of chemical bonds and the formation of new ones.

According to the references, the hardness of the HAp samples is equal to ~14 GPa for amorphous calcium phosphate coatings and ~19 GPa for nanocrystalline HAp coatings. These values correlate with the data reported in [29]. Moreover, Young's modulus of pure titanium grade 4 is ~105 GPa, and shear modulus is ~40 GPa [25].

In the following figures, the results of nanoindentation test are presented:

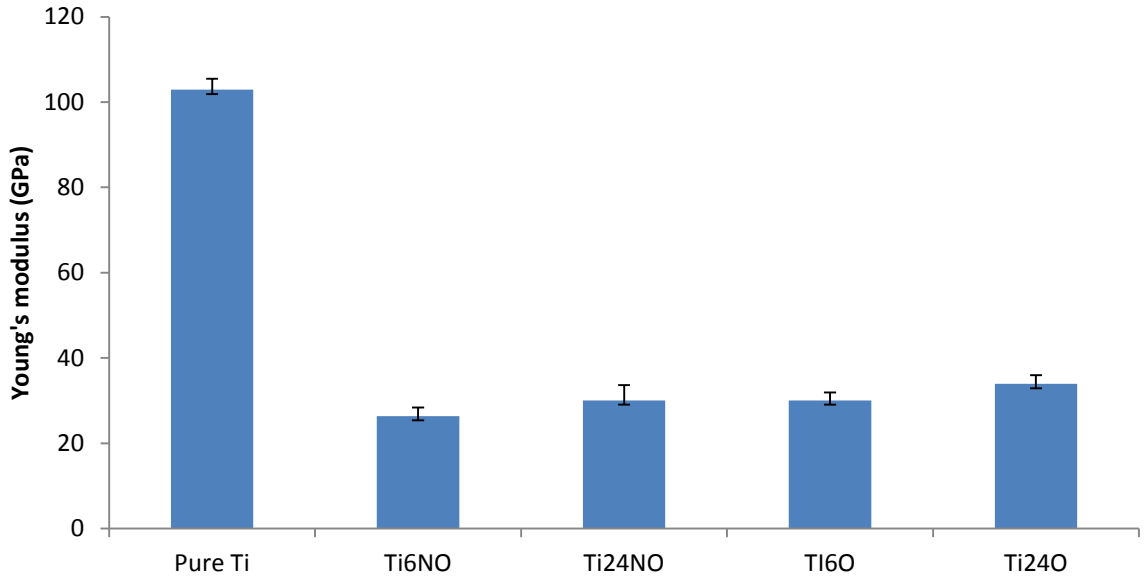

Fig 3.2.1. Young's modulus results

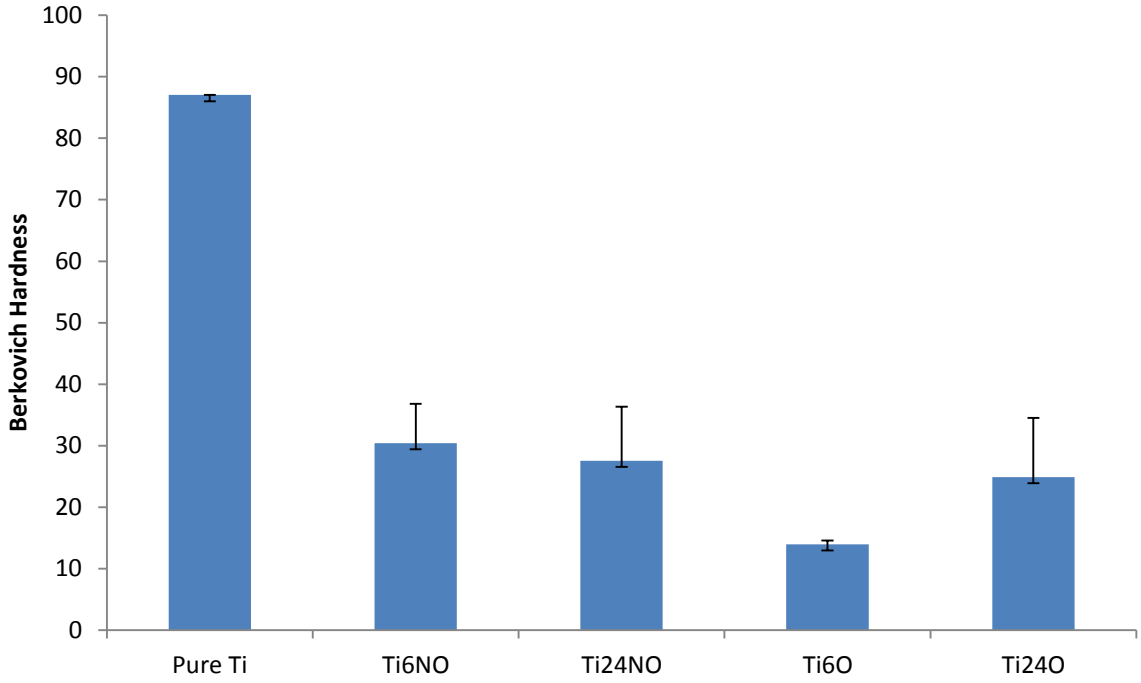

Fig 3.2.2. Berkovich hardness results

It can be seen that Young's modulus of pure Ti obtained is in the order of the referred value in the literature, of about 100 GPa [25]. In addition, the values in all the samples with HAp coatings differ according to the values of the bibliographic references. Figure 3.2.1 presents a Young's modulus value higher for all the coatings. These differences could be possible because in these results, a different coating crystallinity is obtained that which is reported in the papers.

On the other hand, Young's Modulus in Ti6NO is the lowest value comparing with the others conditions. However the hardness is the highest value and this is possible due to the presence of non-metals. Moreover, a large fraction of the indentation deformation is elastic, so the two properties are not truly independent.

Regarding the Young's Modulus, the values are in the same order for coated samples getting the highest value in Ti24O.

In other words, the Young's modulus is reduced in the HAp coating when the hydrothermal treatment is 6 hours. However, when the sample is treated in 24 hours, the Young's modulus is higher. Besides that, in presence of oxide layer, the Young's Modulus increases, independently of time.

The plastic deformation is interpreted in terms of the cluster representation of the hydroxyapatite structure and amorphous calcium phosphates of the same elemental composition and cluster boundary sliding during the deformation. It means that the deformation in the samples treated in 24 hours is lower and the structure of the layer is less likely to break.

Regarding to hardness, the results show that the value of TI6NO is the highest, following by the values of TI24NO and TI24O. TI6O has the lowest value, i.e. lowest resistance of the coating. Comparing those results with the literature, it is seen that with this experimental method gets a higher hardness since the values found in the literature are in the order of ~5 GPa [30].

However, since the modulus of the natural bones is relatively low (7–25 GPa), an implant with high modulus will potentially bring about stress shielding effect, which weakens the bone and deteriorate the implant/bone interface over time [30]. Then, our results are show a small value of elastic modulus, so in future works the influence of coatings with a higher Young's modulus on the bone should be studied.

Then, it could be said that the presence of the coating reduces Young's modulus and hardness comparing with pure titanium. While Young's Modulus increases in presence of the coating, hardness decreases but it remains in the same order.

3.2.2. Bending

Due to the resources that were available, this test was carried out in bars of 32 mm in length and 4 mm in diameter. The conditions chosen for the layer were 24 hours with the presence of titanium oxide, since evaluating the results from the physical-chemical characterization of the coating was considered to be the most favourable. In figures 3.2.3 and 3.2.4, the results obtained from this test are presented:

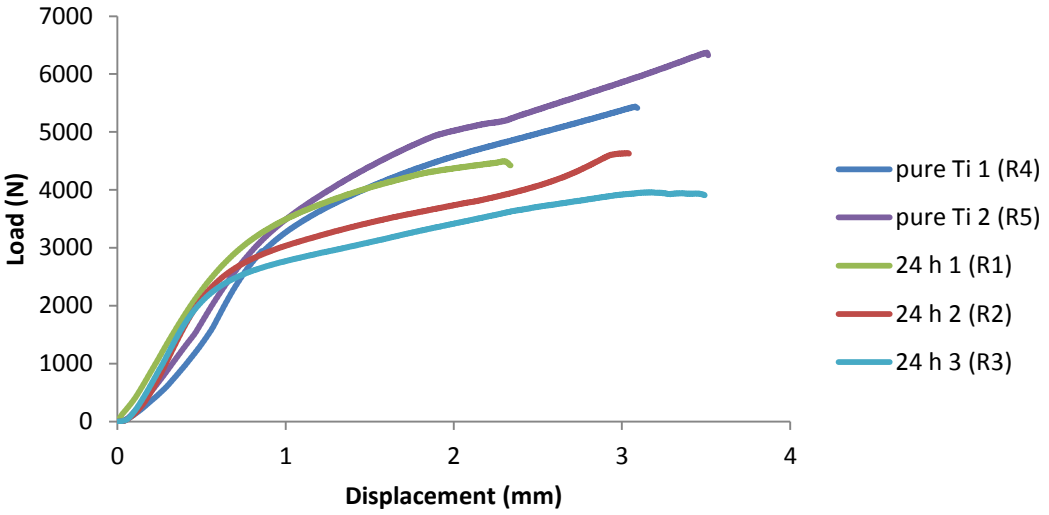

Fig 3.2.3. Relation between force applied and displacement

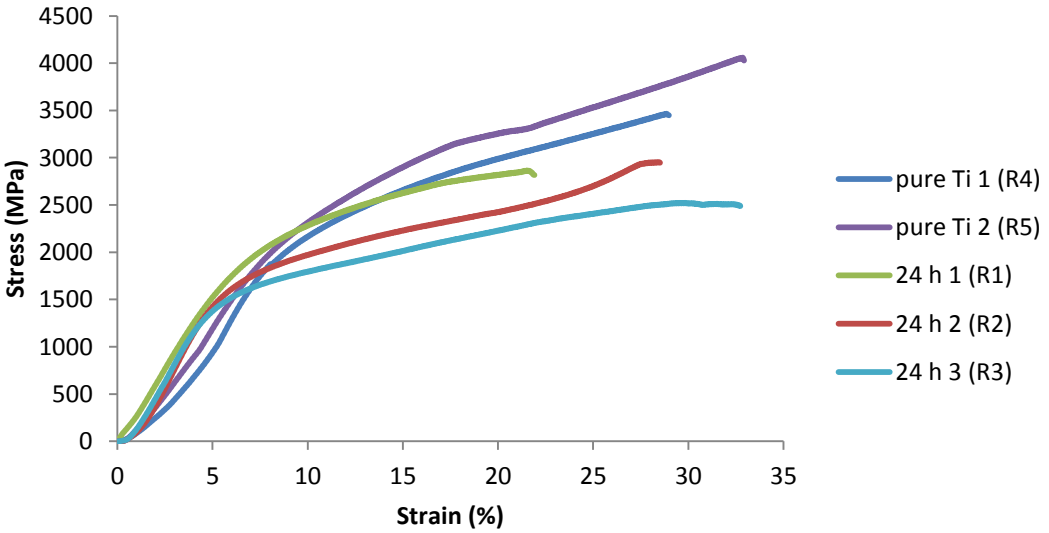

Fig 3.2.4. Relation between stress and strain

As it can be seen in the results presented in figure 3.2.3, the elastic limit zone in coated rods is until around 2 kN and for pure Ti is about 3 kN. Then it can be concluded that in the presence of the coating, the elastic limit is reduced, so that the resistance of the coating is reduced.

In figure 3.2.5 a representation of the test is shown:

Fig 3.2.5. Bending test in R4

Taking into account that the objective of this part is to compare experimentally and numerically the Young's Modulus in pure and coated titanium the Young's modulus is calculated using the following standard formula:

$$\frac{dL}{d\Delta l} = \frac{48 * E * I}{s^3} \qquad \text{(eq. 5)}$$

where $I = \frac{\pi}{4} r^4$ is the moment of inertia; L= Load (N); Δl= displacement (mm); E= Young's Modulus (MPa); s=support span (mm).

Table 8. Experimental values of Young's modulus in pure titanium and in coated titanium

	Pure Ti 1 (R4)	Pure Ti 2 (R5)	24 h 1 (R1)	24 h 2 (R2)	24 h 3 (R3)
Slope	3698,24	3860,09	3636,69	3501,27	3103,56
Moment of Inertia (mm^4)	12,56	12,56	12,56	12,56	12,56
Load at yield point (N)	3070	3200	2495	2185	1909
Displacement at yield point (mm)	0,83	0,82	0,56	0,54	0,45
Stress at yield point (MPa)	1620	1563	1553	1348	1229
Young's Modulus (GPa)	25,13	26,23	24,71	27,79	21,09

It is possible to see that the values of Young's modulus in pure Ti (25GPa) are far from what we expected from the literature (100GPa). This error could be due to the deformations of the supports, since in the experimental test; at the end of the test they have a deformation in the middle of the rod.

Then, it can be observed that there is no difference in the values between pure titanium and coated rods. This is logical because the nanocoating is too small and the effect it can't be measured.

3.2.3. FE Modelling

In this part, simulations have been done in a pure titanium rod and a coated titanium rod. The results are presented in the following figures for pure titanium:

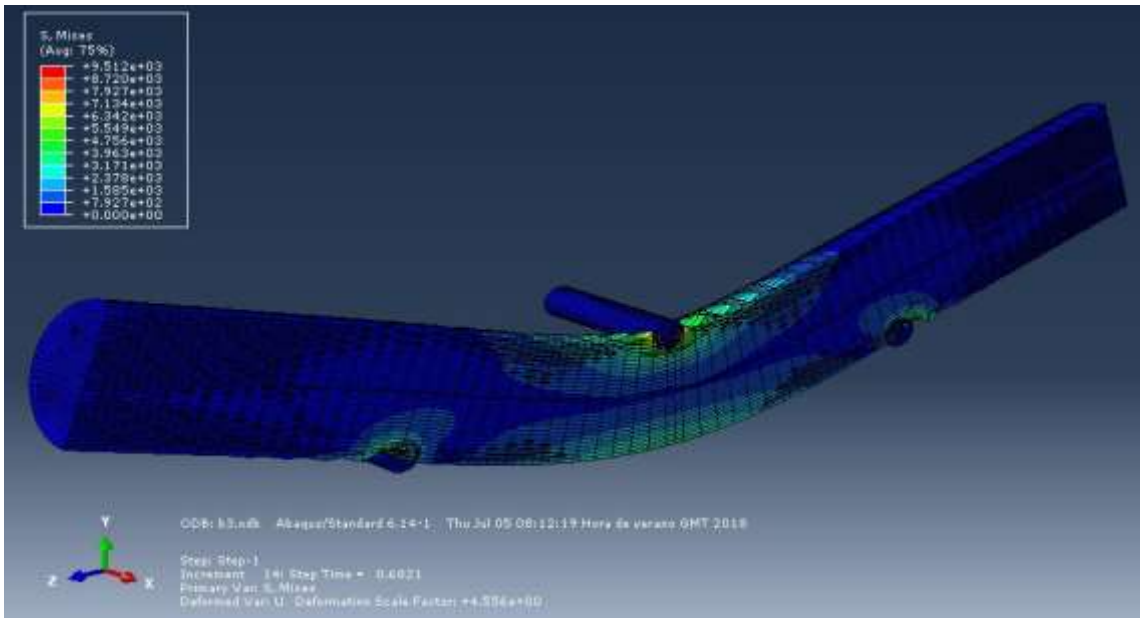

Fig 3.2.6. Stress distribution in pure titanium rod

In figure 3.2.6 for the simulation of the rod without coating and it is obtained a stress distribution in the order of what it expected. The maximum stress value is 9512 MPa, which is a very far from the experimental test, but this value is only obtained in the contact zones. If we assume that the stress should be symmetrical, taking the stress from the lower part of the main rod, the stress is 1585 MPa, which is in the order of the experimental value in the elastic zone (1500 MPa).

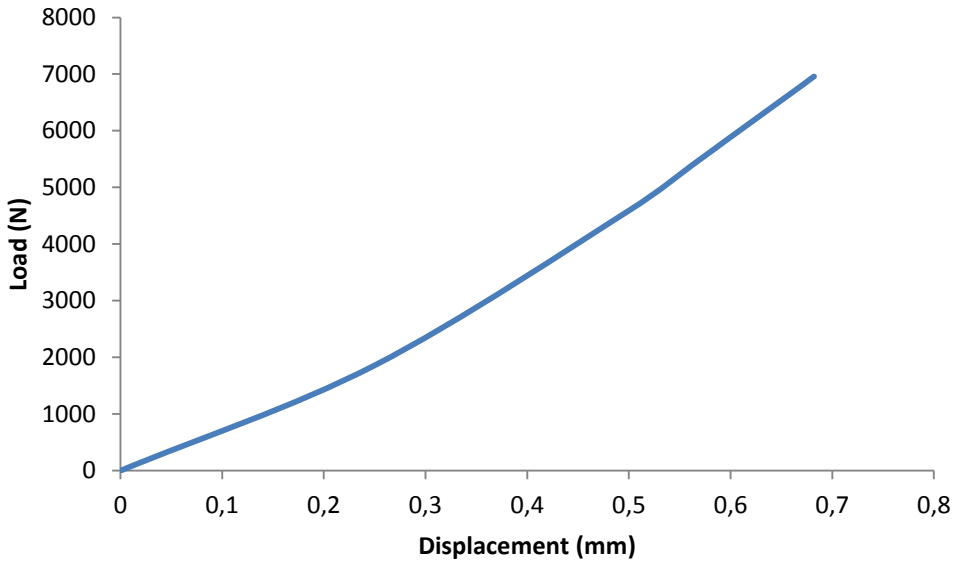

Fig 3.2.7. Load-displacement plot in pure Ti rod from finite element analysis

Numerically in figure 3.2.7, the value obtained for the Young's Modulus is 70GPa in pure titanium, which doesn't match with the experimental value (25GPa) and it also differs from the reported value (100GPa). The stress obtained is in the order of the experimental value.

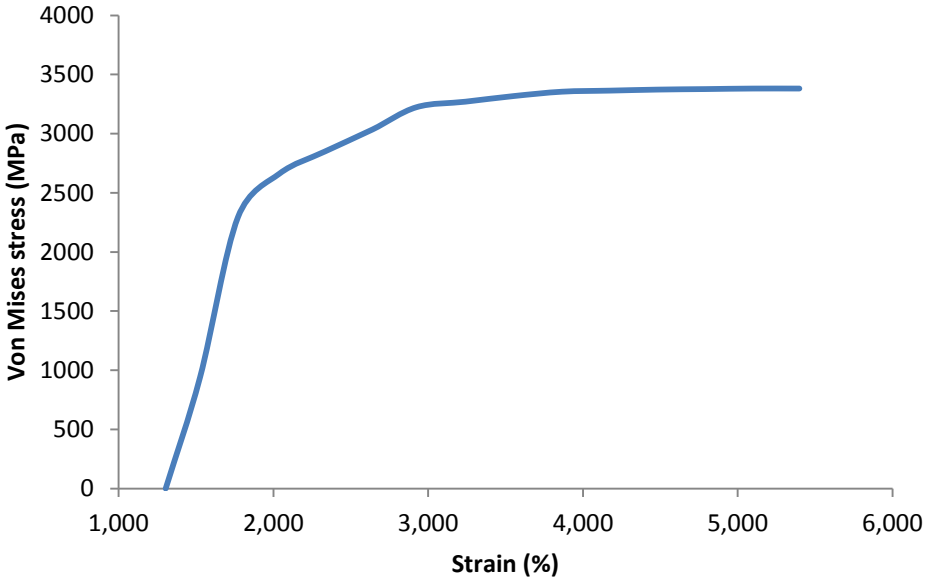

Fig 3.2.8. Von Mises stress- strain plot in pure Ti rod from finite element analysis

On the other hand, the simulated coating was defined with the Young's modulus obtained from the literature. The thickness defined for the coating was 100µm.

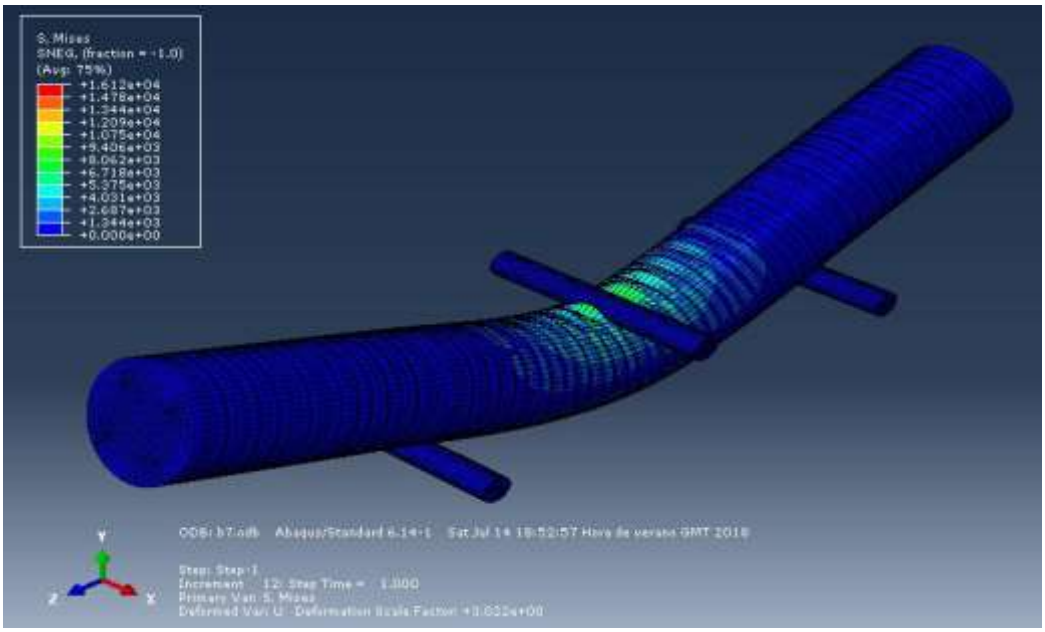

Fig 3.2.9. Stress distribution in a coated rod by finite element analysis

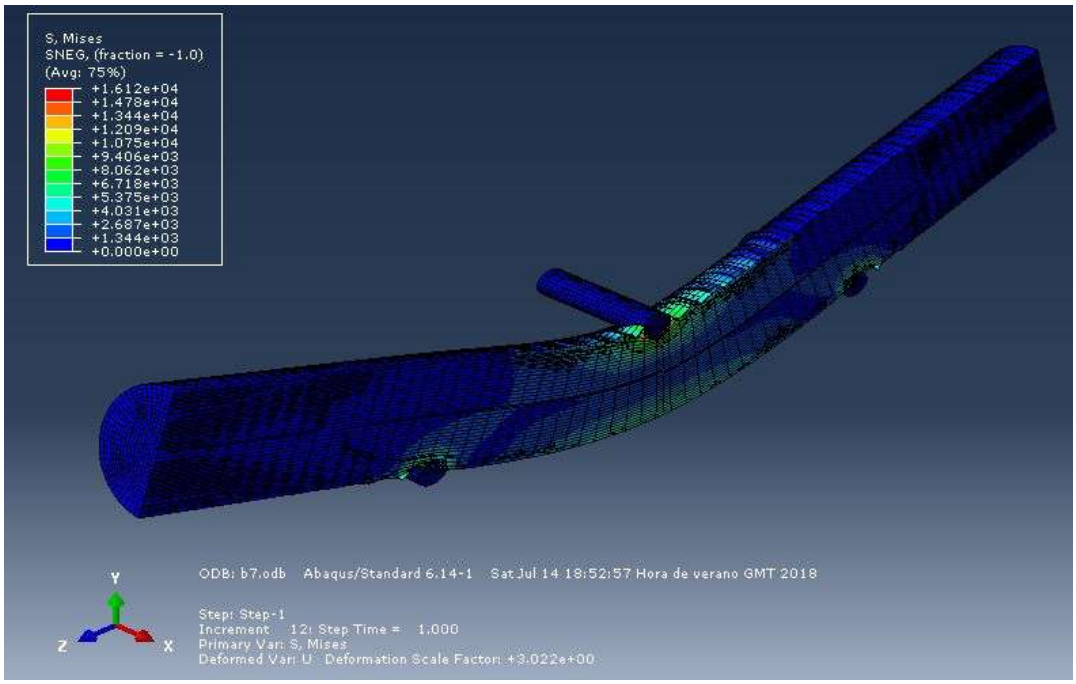

Fig 3.2.10. Half view of stress distribution in the coated rod by finite element analysis

Regarding to figure 3.2.9, the maximum stress obtained is 16120 MPa, which is very far from what it expected, since the value obtained numerically is about 1300 MPa. As it was explained before, taking the stress in the lower part of the main rod, is possible to define the stress as 2687 MPa. It is observed that the experimental and numerical values don't correspond to each other, which could be due to the thickness of elements that was used.

Comparing the plot in figure 3.2.11 obtained with FEA and the plot in figure 3.2.3 experimentally, they are very similar. Yield occurs at a similar force.

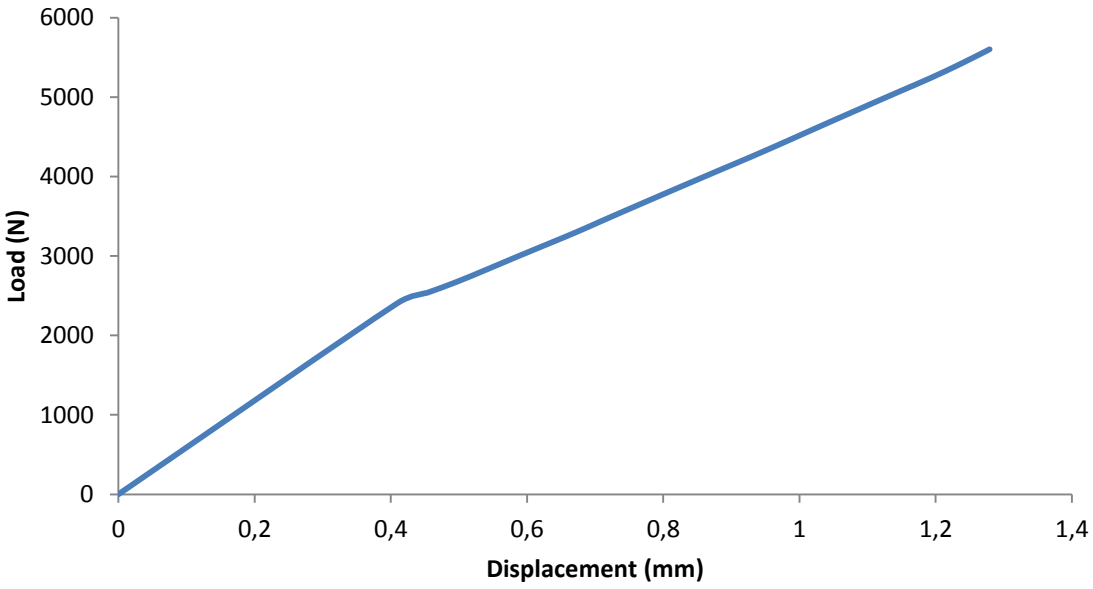

Fig 3.2.11. Load-displacement plot in coated Ti rod from finite element analysis

Evaluating Young's Modulus for coated Titanium with FEA, a value of 27 GPa is obtained. This value match well with the results obtained numerically.

However, the stress obtained in FEA is much higher than experimentally. Maybe this is due to the thickness of shell elements, since it has been imposed a higher thickness in FEA compared with estimated thickness of film, due to computational errors. Another possibility of error is the contact interaction between the top rod and the main rod.

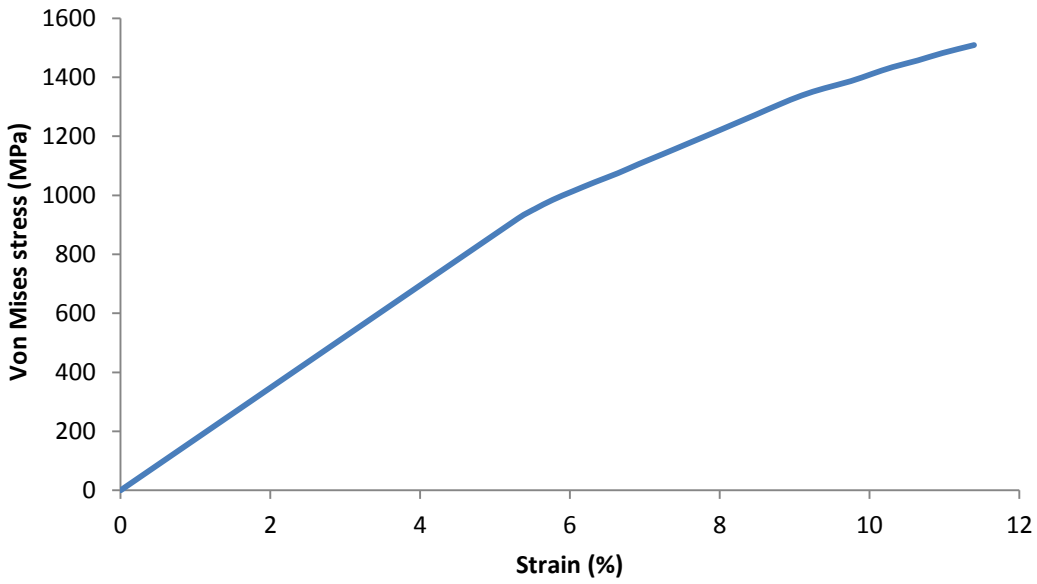

Fig 3.2.12. Stress-strain plot in coated Ti from finite element analysis

Regarding to stress distribution, the values obtained are in the range of the literature, since the most of the stresses that were mainly concentrated at the connection of the abutment-screw-implant complex, especially in tissue-leveled implant (1203.04 MPa) [23].That is that if the connection can support this stress, the coating should have the same mechanical reaction.

It can be assumed then, although the numerical and experimental results differ in the value of pure titanium, in the case of the coated samples there is good agreement. Then the Young's modulus in coated titanium is reduced from pure titanium, and the stress distribution obtained with the oxide layer is lower, so that its elastic limit is lower and will have lower strength than pure titanium. The errors in the numerical may be due to the geometry of the punch in the experimental test and the deformation of the supports in the experimental test too. In addition, the thickness of the supports is not considered in this model, and then it could be a possible source of error.

4 CONCLUSIONS AND FUTURE WORK

Contents

4.1 Conclusions .....

4.2 Future work .....

4.1. Conclusions

In the current work, many samples have been treated in order to evaluate HAp layers for different conditions. Calcium phosphate coatings were formed easily on titanium surface during hydrothermal treatment at 180 °C during 6 and 24 hours. The results have been analyzed according to the influence of the presence of oxide layer and the time in the hydrothermal process.

With XRD, SEM, ATR-FTIR analysis, it was determined thatCaP coatings were deposited in the surface of the titanium with a thickness of 100 nm, which is a great improvement in terms of obtaining a nanostructure layer. It can be confirmed that such is a HAp coating due, to the characteristic spectrum of it, but the crystallinity of HAp coating can't not be defined from XRD results. It can be concluded that the thinner coating is obtained, higher adhesion to the surface (lower contact angle), which is seen in sample Ti24O according to SEM results. They show that the coating is well defined when is formed in presence of $TiO_2$and when the time is 24h. This option is the best because the particle size is smaller and well distributed in the surface. It is confirmed that the presence of TiO_2 is favorable, according to the information in the bibliography too. By means of the nanoindentation test, the hardness is reduced in the HAp coating when the hydrothermal treatment is 6 hours. However, when the sample is treated in 24 hours, the hardness is higher or equal than pure titanium.

Therefore, it can be concluded, comparing all the results, that when the coating is produced at 6 hours under hydrothermal conditions, the presence of TiO_2 doesn't affect too much the results, but when the coating is produced at 24 hours, the presence of TiO_2 results in an improvement in the coating properties. Then, in presence of TiO_2 and treated in 24 hours by hydrothermal conditions, the coating is the optimal for the required applications. That is, a nanocomposite coating was observed, which is homogeneous, crack-free and adherent with uniform thickness, that could be considered as a good quality biomaterial for versatile usages.

In this project, a dental implant is simulated in the form of a rod and analyzed numerically and experimentally. Comparing the bending test and simulations using Abaqus software, the simulation of the coating gets a higher stress value, the elastic limit is higher and deformation lower. Limitations exist due to the simplification made on the coating thickness in the finite element model. It is seen that the coating has better response to the bending test than pure titanium.

Regarding to the mechanical properties it is seen that a higher time and the presence of oxide layer, result in a higher Young's modulus. However, the presence of the coating reduces Young's modulus and Berkovich hardness, compared with pure titanium. While Young's Modulus increases in presence of the coating, Berkovich hardness decreases but it remains in the same order.

Young's modulus in titanium coated is reduced from pure titanium, and the stress distribution obtained with the oxide layer is lower, so that its elastic limit is lower and will have lower strength than titanium without coating.

This study showed that titanium prepared in the described way is a very promising substrate to hydrothermally produce good quality HAp coatings, as it is a uniform layer and a very small thickness.

In summary:

- Hydroxyapatite coating was successfully synthesized on titanium by hydrothermal method.
- The results showed that the presence of TiO_2 on titanium is a key factor inducing the growth of hydroxyapatite coating during the synthesis.
- According to SEM/EDS results and ATR-FTIR spectroscopy, HAp particles were present on all produced coatings.
- In presence of TiO_2 and with 24 hours of hydrothermal process, the nanocoating was homogeneous, crack-free and adherent with uniform thickness, smaller particle size and well distributed in the surface
- From modelling results it is possible to corroborate the experimental results. Young's modulus value is reduced in presence of the coating. For a higher treatment time and in the presence of oxide layer, a higher Young's Modulus is obtained

4.2. Future work

- Improve the finite element model of the bending test (e.g. geometry and deformation of the pins); study the stress field, especially at the substrate-coating interface.
- Investigate the biological response of the coating (in vivo study).
- Evaluate the mechanical response of the coating under realistic loadings

References

[1]Martinez Olmedo, M., Iglesias Godino, F., & Fernández Liétor, P. ;*"Corrosion and fracture analysis in screws of dental implants protheses. New coatings"* ; Engineering Failure Analysis, Volume 82, December 2017, Pages 657-665.

[2]Nancy, C., & Rajendran, N. (n.d.). *"Vancomycin incorporated chitosan/gelatin coatings coupled with TiO2–SrHAP surface modified cp-titanium for osteomyelitis treatment" ;* International Journal of Biological Macromolecules, volume 110, (2018) 197-205.

[3]Suchanek, K., Bartkowiak, A., Gdowik, A., Perzanowski, M., Kąc, S., Szaraniec, B.; *"Crystalline hydroxyapatite coatings synthesized under hydrothermal conditions on modified titanium substrates"* ; Materials Science and Engineering, volume 51, (2015) 57-63.

[4]Feng, G., Cheng, X., Xie, D., Wang, K., & Zhang, B. (2015, October 14). *"Fabrication and characterization of nano prims-like hydroxyapatite coating on porous titanium substrate by combined biomimetic-hydrothermal method".* Materials Letters, volume 163, (2016) 134-137.

[5]Jung, U.-W., Hwang, J.-W., Choi, D.-Y., Hu, K.-S., Kwon, M.-K., Choi, S.-H., et al. (n.d.). *"Surface characteristics of a novel hydroxyapatite-coated dental implant" ;* J Periodontal Implant Sci. volume 42, (2012) 59-63.

[6]Kirmanidou, Y., Sidira, M., Drosou, M.-E., Bennani, V., Bakopoulou, A., Tsouknidas, A., et al. (n.d.). *"New Ti-Alloys and Surface Modifications to Improve the Mechanical Properties and the Biological Response to Orthopedic and Dental Implants: A Review".* Hindawi, BioMed Research International volume (2016) 21.

[7]Kay, J., Golec , T., & Riley , R. "*Hydroxyapatite-coated subperiosteal dental implants: design rationale and clinical experience".* The Journal of Prosthetic Dentistry, Volume 58, Issue 3, September 1987, Pages 339-343

[8]Mohan, L., Manivasagam, G., Dhinasekaran, D., Sankara Narayanan, T., & Asokamani, R. (2011, December 31). *"Electrophoretic deposition of nanocomposite (HAp + TiO2) on titanium alloy for biomedical applications".* Ceramics International, volume 38, (2012) 3435-3443.

[9]Block, M., Kent, J., & Kay , J. *"Evaluation of hydroxyapatite coated titanium dental implants in dogs".* Journal of Oral and Maxillofacial Surgery Volume 45, Issue 7, July 1987, Pages 601-607.

[10]Cook, S., Kay, J., Thomas , K., & Jarcho, M. *"Interface mechanics and histology of titanium and hydroxylapatite-coated titanium for dental implant applications".* Int J Oral Maxillofac Implants. 1987;2(1):15-22.

[11]Golec, T., & Krauser , J. *"Long-term retrospective studies on hydroxyapatite coated endosteal and subperiosteal implants".* Dent Clin North Am. 1992 Jan;36(1):39-65.

[12]Ou, S.-F., Lin, C.-S., & Pan, Y.-N. *"Microstructure and surface characteristics of hydroxyapatite coating on titanium and Ti-30Nb-1Fe-1Hf alloy by anodic oxidation and hydrothermal treatment".* Surface & Coatings Technology 205 (2011) 2899–2906.

[13]Yang, S., Lee, S., Bajpai , I., & Kim, S. *"Hydrothermal treatment of Ti surface to enhance the formation of low crystalline hydroxyl carbonate apatite".* Biomaterials Research, (2015) 19-4.

[14]Parnia, F., Yazdani, J., Javaherzadeh , V., & Maleki Dizaj, S. *"Overview of Nanoparticle Coating of Dental Implants for Enhanced Osseointegration and Antimicrobial Purposes".* J Pharm Pharm Sci. 2017;20(0):148-160.

[15]Jiang, W., Wang, W., Shi, X., Chen, H., Zou, W., Guo, Z., y otros. (s.f.). *"The effects of hydroxyapatite coatings on stress distribution near the dental implant-bone interface".* Applied Surface Science 255 (2008) 273–275

[16]Herekar, M., Patil, V., Mulani, S., Sethi, M., & Padhye, O. (s.f.). *"The influence of thread geometry on biomechanical load transfer to bone: A finite element analysis comparing two implant thread designs".* Dent Res J (Isfahan). 2014 Jul-Aug; 11(4): 489–494.

[17]Asgharzadeh Shirazi, H., Ayatollahi, M., & Asnaf, A. (s.f.). *"To reduce the maximum stress and the stress shielding effect around a dental implant–bone interface using radial functionally graded biomaterials".* Computer methods in BiomeChaniCs and BiomediCal engineering, 2017 Vol. 20, no. 7, 750–759

[18]*Geometrical instrumentation and analysis X-Ray*. Retrieved from https://serc.carleton.edu/research_education/geochemsheets/techniques/XRD.html (08-02-2018)

[19]*rruff.info*. (n.d.). Retrieved from http://rruff.info/Anatase/R060277 (15-05-2018)

[20]*Geometrical instrumentation and analysis SEM*. Retrieved from https://serc.carleton.edu/research_education/geochemsheets/techniques/SEM.html (24-06-2018)

[21]*Thermo Fisher Scientific*. Retrieved from https://www.thermofisher.com/pt/en/home/industrial/spectroscopy-elemental-isotope-analysis/spectroscopy-elemental-isotope-analysis-learning-center/molecular-spectroscopy-information/ftir-information/ftir-sample-handling-techniques/ftir-sample-handling-tec

[22]Yuan, Y., & Randall Lee, T. *"Contact Angel and Wetting Properties".*Surface Sciences, volume 51, 3-34.

[23] Chang, H.-S., Chen, Y.-C., Hsieh , Y.-D., & Hsu, M.-L. (s.f.). *"Stress distribution of two commercial dental implant systems: A three-dimensional finite element analysis".* Journal of Dental Sciences (2013) 8, 261e271

[24]Hedia, H. (s.f.). *"Effect of coating thickness and its material on the stress distribution fordental implants".* Journal of Medical Engineering & Technology, volume 31 (2007) 280-287

[25]*Aerospace specification metals*. Retrieved from http://asm.matweb.com/search/SpecificMaterial.asp?bassnum=mtu040

[26] A. Martins, M., Santos, C., Almeida, M., & V. Costa, M. (s.f.). *"Hydroxyapatite micro- and nanoparticles: Nucleation and growth mechanisms in the presence of citrate species".* Journal of Colloid and Interface Science 318 (2008) 210–216.

[27]Ferraris, S., Vitale, A., Bertone, E., Guastella, S., Cassinelli, C., Pan, J., y otros. *"Multifunctional commercially pure titanium for the improvement of bone integration: Multiscale topography, wettability, corrosion resistance and biological functionalization".* Materials Science and Engineering, C60 (2016) 384-393.

[28]Rey , C., Combes , C., Drouet , C., Grossin, D., Bertrand, G., & Soullé, J. (2017). "Bioactive Calcium Phosphate Compounds: Physical Chemistry". Elsevier Ltd.

[29]Ievlev, V., Kostyuchenko, A., Darinskii, B., & Barinov, S. (2013, July 10). *"Hardness and Microplasticity of Nanocrystalline and Amorphous Calcium Phosphate Coatings".* Fizika Tverdogo Tela, 2014, Vol. 56, No. 2, pp. 318–325.

[30]Han, C., Li, Y., Wang , Q., Cai, D., Wei , Q., Yang, L., y otros. (s.f.). *"Titanium/hydroxyapatite (Ti/HA) gradient materials with quasi-continuous ratios fabricated by SLM: Material interface andfracture toughness".* Materials and Design 141 (2018) 256–266

[31]Santos, C., Margarida Almeida, M., & Costa, M. *"Morphological Evolution of Hydroxyapatite Particles in the Presence of Different Citrate:Calcium Ratios".* Cryst. Growth Des., 2015, 15 (9), pp 4417–4426.

[32]Schuh, C. (n.d.). *"Nanoindentation studies of materials".* Materialstoday, volume 9, Issue 5, (2006) 32-40.

[33]Caetano-Lopes, J., Margarida Nery, A., Henriques , R., Canhão, H., Duarte, J., Amaral, P., y otros. (s.f.). *"Chronic arthritis directly induces quantitative and qualitative bone disturbances leading to compromised biomechanical properties".* Clinical and Experimental Rheumatology 2009; 27: 000-000.